Published in final edited form as:
Cytoskeleton (Hoboken). 2010 June ; 67(6): 346–364. doi:10.1002/cm.20449.

Novel Interactors and a Role for Supervillin in Early Cytokinesis

Tara C. Smith, **Zhiyou Fang**, and **Elizabeth J. Luna***
Department of Cell Biology and Cell Dynamics Program, University of Massachusetts Medical School, Worcester, MA 01605

Abstract

Supervillin, the largest member of the villin/gelsolin/flightless family, is a peripheral membrane protein that regulates each step of cell motility, including cell spreading. Most known interactors bind within its amino (N)-terminus. We show here that the supervillin carboxy (C)-terminus can be modeled as supervillin-specific loops extending from gelsolin-like repeats plus a villin-like headpiece. We have identified 27 new candidate interactors from yeast two-hybrid screens. The interacting sequences from 12 of these proteins (BUB1, EPLIN/LIMA1, FLNA, HAX1, KIF14, KIFC3, MIF4GD/SLIP1, ODF2/Cenexin, RHAMM, STARD9/KIF16A, Tks5/SH3PXD2A, TNFAIP1) co-localize with and mis-localize EGFP-supervillin in mammalian cells, suggesting associations in vivo. Supervillin-interacting sequences within BUB1, FLNA, HAX1, and MIF4GD also mimic supervillin over-expression by inhibiting cell spreading. Most new interactors have known roles in supervillin-associated processes, e.g. cell motility, membrane trafficking, ERK signaling, and matrix invasion; three (KIF14, KIFC3, STARD9/KIF16A) have kinesin motor domains; and five (EPLIN, KIF14, BUB1, ODF2/cenexin, RHAMM) are important for cell division. GST fusions of the supervillin G2–G3 or G4–G6 repeats co-sediment KIF14 and EPLIN, respectively, consistent with a direct association. Supervillin depletion leads to increased numbers of bi- and multi-nucleated cells. Cytokinesis failure occurs predominately during early cytokinesis. Supervillin localizes with endogenous myosin II and EPLIN in the cleavage furrow, and overlaps with the oncogenic kinesin, KIF14, at the midbody. We conclude that supervillin, like its interactors, is important for efficient cytokinesis. Our results also suggest that supervillin and its interaction partners coordinate actin and microtubule motor functions throughout the cell cycle.

Keywords

cytokinesis; cleavage furrow; supervillin; EPLIN/LIMA1; KIF14

INTRODUCTION

The coordination of motor function with membrane dynamics is of fundamental importance for cell motility and membrane trafficking in interphase cells, as well as for the proper segregation of chromosomes and cytoplasm during cell division (Akhmanova et al. 2009; Glotzer 2005; Hickson and O'Farrell 2008; Hirokawa and Noda 2008; Kunda and Baum 2009). The actin motor, myosin II, which is required for cell adhesion and migration, also regulates membrane trafficking and microtubule dynamics (Chan et al. 2005; Even-Ram et al. 2007; Vascotto et al. 2007; Vicente-Manzanares et al. 2007). Conversely, microtubule motors (kinesins, dynein) coordinate the flow of myosin II regulatory factors to and from the cell periphery during the formation and turnover of cell-substrate adhesions and the

*Correspondence: Elizabeth J. Luna, Ph.D., Department of Cell Biology, Biotech 4, Room 306, 377 Plantation Street, Worcester, MA 01605, Tel: (508) 856-8661, Fax: (508) 856-8774, Elizabeth.Luna@umassmed.edu.

contractile ring (Caviston and Holzbaur 2006; Gimona et al. 2008; Kasahara et al. 2007; Soldati and Schliwa 2006).

The tightly bound membrane protein, supervillin, is a regulatory hub for cytoskeletal, membrane, and signaling proteins. Different combinations of the three actin-binding sites in the supervillin N-terminus either bundle or crosslink actin filaments (Chen et al. 2003). The supervillin N-terminus also promotes myosin II contractility, apparently through its direct binding to the S2 regulatory region of non-muscle and smooth muscle myosin II heavy chains and to the N-terminus of the long (L) form of myosin light chain kinase (L-MLCK) (Chen et al. 2003; Gangopadhyay et al. 2004; Takizawa et al. 2007). The supervillin C-terminus also may promote myosin II-based contractility through binding to calponin, an actin-binding protein that mediates signaling through extracellular-signal-regulated kinases (ERK1/2) (Gangopadhyay et al. 2004). An isoform of supervillin (SmAV) is required for stimulus-mediated contractility and ERK signaling in smooth muscle and co-sediments from this tissue with all members of the ERK signaling scaffold (Gangopadhyay et al. 2009; Gangopadhyay et al. 2004). The non-muscle supervillin isoform also regulates ERK signaling and motile processes, including cell spreading, cell-substrate attachment, and matrix degradation (Crowley et al. 2009; Fang et al. In press; Takizawa et al. 2007; Takizawa et al. 2006). Cytoplasmic “punctae” of non-muscle supervillin contain the Src and ERK substrate, cortactin, and move with velocities characteristic of kinesins, suggesting possible cross-talk with microtubule motors (Crowley et al. 2009; Fang et al. In press). Endogenous supervillin binds tightly to cholesterol-rich “lipid raft” membranes (Nebl et al. 2002), and supervillin knockdown inhibits actin-dependent integrin recycling from peripheral endosomes, consistent with an active role in some vesicle movements (Fang et al. In press). Thus, supervillin function and biochemistry suggest a role in the coordination of membrane-based signaling and motor function.

The name “supervillin” derives from the homology (29% identity, 50% similarity) of its C-terminus to the gelsolin/villin/flightless family of actin- and membrane-interacting proteins, many of which have both cytoskeletal and nuclear functions (Archer et al. 2005). However, the supervillin C-terminus is structurally distinguishable (Pestonjamasp et al. 1997; Pope et al. 1998). The divergence from gelsolin, villin, and flightless appears to be evolutionarily ancient, with orthologs of supervillin apparent in fly and worm genomes, *e.g.* CG33232 in *D. melanogaster* and C10H11.1 in *C. elegans* (Pestonjamasp et al. 1997). As has been proposed for flightless (Claudianos and Campbell 1995), supervillin may have arisen from an insertion within the first gelsolin/villin domain repeat (G1) in a primordial villin-like gene. G1 sequences are replaced by the unique supervillin N-terminus, with a notable absence of the residues in gelsolin and villin G1 domains that bind, cap, and sever actin filaments (Burtnick et al. 1997; Pestonjamasp et al. 1997). Supervillin-specific residues also replace 73% (11/15) of the residues in gelsolin domains G4 and G6 that contact actin, consistent with the observed inability of the supervillin C-terminus to localize with cytoskeletal actin (Robinson et al. 1999; Wulfkuhle et al. 1999). Similarly, although the extreme supervillin C-terminus folds like the “headpiece” domain of villin, the supervillin headpiece exhibits a different pattern of surface charges and lacks F-actin binding activity (Brown et al. 2009; Vardar et al. 2002).

We hypothesized that the evolutionarily conserved differences that distinguish supervillin from gelsolin and the other gelsolin/villin family members contain interaction domains for unique binding partners. The only interaction partners currently known for the supervillin C-terminus are the androgen and estrogen receptors, which bind N-terminal to the G2–G6 repeats in supervillin (Ting et al. 2002), and calponin, which binds within the C-terminal 251 supervillin residues (Gangopadhyay et al. 2004). We report here that supervillin-specific loops apparently extend from the gelsolin-like repeats in the supervillin C-terminus and

identify 12 new candidate interactors for these and other C-terminal sequences, based on yeast two-hybrid screens and classifier assays in mammalian cells. The new interactors include oncogenes, tumor suppressors, and 3 proteins with kinesin motor domains. We confirm interactions between supervillin and two of these proteins—the oncogenic kinesin, KIF14, and the tumor suppressor protein, EPLIN/LIMA1. Because these proteins and other newly described supervillin interactors play a role in cell division, we examined supervillin knockdown cells for a defect in this process. We found that supervillin does play a role during early cytokinesis, possibly through interactions involving EPLIN or KIF14. We suggest that these results functionally validate our interaction screens and provide many new testable hypotheses for the roles of the supervillin interactors in motile processes. Our results further suggest that supervillin-based scaffolds of interactors coordinate membrane interactions with actin and microtubule motors during both cell division and interphase.

MATERIALS AND METHODS

Molecular Modeling

Structural alignments of human supervillin (NP_003165) sequences with domains within human gelsolin (NP_000168) were performed using SWISS-MODEL (http://swissmodel.expasy.org) (Arnold et al. 2006). Sequences were oriented and colored using Swiss-PdbViewer (DeepView), v4.0 (http://spdbv.vital-it.ch/). Supervillin amino acids 1326–1699 were automatically aligned with gelsolin repeats 4 through 6 (G4–G6, amino acids 445–765; PDB: 2FH1B) (Chumnarnsilpa et al. 2006). Additional structural elements in supervillin residues 1019–1306 were aligned with gelsolin repeats 2 and 3 (G2–G3) and the G3–G4 linker (gelsolin amino acids 189–444; PDB: 2FGHA) (Urosev et al. 2006) in forced comparisons. No alignments could be generated between supervillin sequences 830–1019 and elements in gelsolin repeat 1 (G1).

Plasmids

EGFP-C1 and EGFP-tagged bovine supervillin (EGFP-SV) vectors were described previously (Wulfkuhle et al. 1999). GFP-tagged ITGB3BP (β3-endonexin, NRIF3) was generously provided by Dr. Mark Ginsberg (University of California, San Diego) (Shattil et al. 1995). HA-tagged wild type (WT) and dominant negative (DN) RHAMM constructs were kind gifts from Dr. Eva Turley (London Health Sciences Centre, Ontario, Canada) (Hall and Turley 1995). A Flag-tagged construct encoding EPLINα was the generous gift of Dr. Raymond S. Maul (University of California, Los Angeles) (Song et al. 2002). The EGFP-KIF14 plasmid was kindly supplied by Dr. Michael Carleton (Merck Research Laboratories, Seattle, WA) (Carleton et al. 2006).

The sequence encoding bovine supervillin amino acids 834-1291 (SV834-1291) was obtained by PCR using the sense primer 5′-GGTACCACCAGACATGCAGTTAGAGTCGGACC and the antisense primer, 5′-CTCGAGGTCACGTCGTAAGGCTTGACCTCTG. Sequence encoding SV1008-1791 was obtained by PCR using the sense primer 5′-GGTACCAGAACAGAATTCCAACAACAGTGCAG, and the antisense primer 5′-ACTCGAGAGAACAGACCTTTCGCTTTCTTCAG. Both PCR products were ligated in-frame into the pHybLex/Zeo bait vector using KpnI and XhoI, end sequenced, and tested for self-activation. The bait vector encoding SV834-1291 was mutated at amino acids 851 and 852 using the QuickChange kit (Stratagene, La Jolla, CA), with the sense primer 5′-AGGCTGGAAACCT**c**CC**c**AAGAAGGCTGAATA, and antisense primer 5′-TATTCAGCCTTCTT**g**GG**g**AGGTTTCCAGCCT, and separately mutated at amino acids 952 and 953 using the sense primer 5′-GAGGGAAGATC**a**CC**c**GCAGGAGTACACTGA, and the antisense primer 5′-TCAGTGTACTCCTGC**g**GG**t**GATCTTCCCTC. Mutations

(shown in bolded lower case) were confirmed by sequencing, and baits were re-tested for self-activation before screening of the preys.

GST plasmids containing supervillin C-terminal sequences were constructed from restriction digests of pEGFP-SV. The gelsolin/villin homology domains were transferred in frame into GST vectors (pGEX-6P series, GE Healthcare, Piscataway, NJ) as follows: SV1009-1398 was restricted with EcoRI and SalI and ligated into pGEX-6P-3; SV1398-1792 was restricted with SalI and NotI and ligated into pGEX-6P-2. All vectors were verified by end sequencing.

Antibodies

For immunofluorescence, tubulin was visualized with mouse monoclonal antibody, clone TUB2.1 (Sigma-Aldrich, St. Louis, MO) and goat anti-mouse Alexa Fluor 568 antibody (Invitrogen, Carlsbad, CA). Rabbit antibodies used for immunofluorescence were affinity-isolated monoclonal (71D10) anti-myc (Cell Signaling, Beverly MA); affinity-isolated anti-HA and affinity-purified polyclonal anti-Flag (Sigma); affinity purified polyclonal anti-myosin IIA (Covance, Berkeley, CA); and affinity-purified anti-KIF14 (Cat#A300-912A, Bethyl Laboratories Inc., Montgomery, TX). Rabbit anti-EPLIN was the kind gift of Dr. Raymond S. Maul (University of California, Los Angeles). Rabbit antibodies were visualized with goat anti-rabbit Alexa Fluor 568 (Invitrogen). Mouse anti-GFP (clones 7.1 and 13.1; Roche, Mannheim, Germany) and goat anti-mouse Alexa Fluor 488 were used to enhance visualization of EGFP-SV in stably expressing HeLa cells. Supervillin and β-actin were visualized on immunoblots with affinity-purified H340 rabbit antibody (Nebl et al. 2002; Oh et al. 2003) and monoclonal anti-actin (C4, Millipore, Billerica, MA), respectively, and goat anti-rabbit-HRP or anti-mouse-HRP (Jackson ImmunoResearch, West Grove, PA). GST was visualized with goat polyclonal anti-GST (GE Healthcare) and donkey anti-goat-HRP (Jackson ImmunoResearch).

Yeast Two-Hybrid Screens

Yeast two-hybrid screens were performed using the Hybrid Hunter system (Invitrogen), as described previously (Chen et al. 2003; Takizawa et al. 2006). In brief, a HeLa cDNA library of 1.03×10^7 primary transformants was covered twice with each bait. For SV834-1291, large colonies grown on induction medium were picked after 24 hr and tested for β-galactosidase activity and leucine autotrophy. Of 600 initial colonies, the 33 that passed these tests were segregated, sequenced, and confirmed in a directed screen against the original bait, yielding 20 unique preys encoding 19 distinct protein sequences. These preys were further screened in directed assays against the SV834-1291 bait carrying mutations either at amino acids F851S and L852P or at L952H and L953P. Because yeast containing SV1008-1791 grew slowly, large colonies were picked for up to 96 hr. Of 115 initial colonies with this bait, 40 were segregated, sequenced, and confirmed as above, yielding 13 unique preys encoding 10 different proteins. All sequences were then reciprocally screened against the other bait. Nonspecific interactions were eliminated in a directed screen with pHybLex/Zeo, the empty bait vector.

Prey sequences encoding the following proteins (inclusive amino acids) were moved to a modified pCMV-myc vector (Clontech, Mountain View, CA) using HindIII and XhoI, as described previously (Takizawa et al. 2006): EPLINβ(650–759), KIF14(1522–1648), FLNA(987–1186 and 2169–2414), KIFC3(237–366), Tks5(318–655), TNFAIP1(119–316), MIF4GD(122–256), ART-27(1–157), STARD9(2528–2663), PCNXL3(365–548), CENPF(2378–2516), NM23B(1–152), ODF2(133–269), PAN3(229–600), MPHOSPH9(673–858), KIF22(488–665), and ATRX(97–292). Other prey sequences were moved to a pCMV-HA (Clontech) vector using KpnI and NotI: HSP90(11–241),

HAX1(144–279), BUB1(4–313), MKL2(382–692), and MLL(968–1206). All were confirmed by end sequencing.

Cells, Transfections, and Imaging

COS7-2 cells were grown for ≤ 20 passages in Dulbecco's modified Eagle high glucose media (DMEM-HG, GIBCO #11995, Invitrogen) supplemented with 10% fetal calf serum (FCS). HeLa S3 Tet-Off cells (HeLa cells, Clontech) were grown for ≤ 20 passages in DMEM-HG supplemented with 10% FCS, non-essential amino acids, and 2 mM L-glutamine. For spreading assays, HeLa cells in a 6-well plate were transfected with 0.5 μg/well of plasmids encoding myc- or HA-tagged prey sequences using Lipofectamine 2000 (Invitrogen). Cells were lifted with trypsin/EGTA after 24 hr, plated on coverslips pre-coated with 10 μg/ml fibronectin, and fixed with 4% paraformaldehyde after spreading for 30 min; cells were defined as "spread" when their longest diameter exceeded twice the average diameter of initially plated cells (Takizawa et al. 2007). For co-localization and mis-localization assays, COS7-2 cells in a 6-well plate were transfected with Effectene (Qiagen, Valencia, CA) for 24 hr with 1 μg/well of EGFPSV1-1792 and 0.5 μg/well of each prey mammalian expression plasmid. Cells were then fixed, permeabilized with 0.1% Triton X-100 for 3.5 min, and stained for immunofluorescence (Takizawa et al. 2006). HeLa cells stably expressing a GFP fusion to human supervillin were synchronized by double thymidine block, as described (Harper 2005), and used for immunolocalization with endogenous myosin II, EPLIN, and KIF14. Depending on the experiment, cells were stained for myc (1:200 dilution), HA (1:200), EGFP (1:200), myosin IIA (1:100), EPLIN (1:200), or KIF14 (1:100). F-actin was visualized with phalloidin labeled with Alexa Fluor 488 or Alexa Fluor 350 (Invitrogen). Slides were analyzed with a 40X (NA 0.9) or 100X (NA 1.3) Plan-NeoFluor oil immersion objective on a Zeiss Axioskop fluorescence microscope, a RETIGA 1300 CCD camera (QImaging, Surrey, BC, Canada), and OpenLab 3.5.2 software (Improvision, Waltham, MA). Images were adjusted uniformly for contrast and brightness, and merged images were assembled using Adobe Photoshop software.

For RNAi, HeLa cells were transfected with Stealth RNA (Invitrogen) duplexes (dsRNA) targeting the following sense nucleotides in the human supervillin cDNA sequence: (1) 1680–1704: 5′-CAGCCATAAGGAATCTAAATATGCT-3′ (Takizawa et al. 2006); (2) 2472–2496: 5-CCCCUGGAAGAUAUCGAAGCCAGAC-3′ (Takizawa et al. 2006); or (3) 6016–6040: 5′-TATTAAGGTAGAAAGGTTGATTCGC-3′ (3′-UTR). The Stealth duplex sequences 5′-CAGAAUAAAGGAUCUAUAAUCCGCU-3′ and 5′-GAACUAUGAAGGACCACCAGAGAUA-3′ were used as controls (Takizawa et al. 2006). HeLa cells at ~30% confluence were transfected with 20 nM dsRNA and Lipofectamine 2000 (Invitrogen), according to the manufacturer's instructions. Depending on the experiment, cells were either assayed within 3 days of transfection or were split 1:3 after 2 days of growth, re-transfected 8–10 hr after splitting, and used within another 36–40 hr of growth (Takizawa et al. 2006).

Confocal Z-sections were obtained with a 60X Plan Apo objective lens (N.A. 1.4) on a Nikon TE-2000E2 inverted microscope (Nikon Instruments, Melville, NY) with a Yokogawa CSU10 Spinning Disk Confocal Scan Head (Solamere Technology Group, Salt Lake City, UT), Rolera-MGi Plus camera (QImaging), and MetaMorph 7.6 software (MDS Analytical Technologies, Downington, PA). Time-lapse images of unsynchronized HeLa cells in an enclosed chamber at 37°C were acquired every 3 min for 16–24 hr with a 10X objective lens (NA 0.30) and a 1.5X tube lens on a DMIRE 2 inverted microscope with a mechanical stage (Leica Microsystems, Bannockburn, IL), a Retiga Exi cooled CCD camera (QImaging), and SimplePCI software (Hamamatsu Corp., Sewickley, PA). Metaphase was defined morphologically by the alignment of sister chromatids in the center of the cell, anaphase by chromatid separation to opposite poles, telophase/early cytokinesis by the

appearance of the cleavage furrow or an initial membrane invagination, and late cytokinesis by the presence of two daughter cells connected by an intracellular bridge. Movies were exported for each field of cells as AVI files and processed using OpenLab 3.5.2 software to enhance contrast in selected regions of interest.

Scoring for EGFP-supervillin distributions and appearance

Micrographs of COS7-2 cells expressing EGFP-SV, either alone or in combination with myc- or HA-tagged proteins, were taken using identical exposure times and adjusted uniformly using Adobe Photoshop software. The images were classified first by the distribution and intensity of staining of the EGFP signal into three categories: predominantly central, predominantly edge, or balanced between both locations. The same images were further classified by the appearance of the EGFP-SV signal as predominantly punctate, predominantly fibrous, or equivalent distribution to both types of structures. The rounding effect on cell morphology was tabulated from these images and from control images taken of cells expressing myc- or HA-tagged proteins alone after staining with Alexa Fluor 488 phalloidin (Invitrogen). Margins of error in these classifications were calculated to be between 13% and 16% at the 90% confidence interval using the random sample calculator found at www.custominsight.com/articles/random-sample-calculator.asp. Only differences from the controls of >17% were considered positive.

Growth Curves and Cytokinesis Failure

HeLa cells stably expressing a control or SV-specific short-hairpin RNA (shRNA) were passaged into 6-cm dishes at 0.2×10^5 per dish and incubated under normal growth conditions. Plates were trypsinized up to 70 hr after plating, and cell numbers were calculated using a hemacytometer at the time points indicated. Separate plates were used to assay the amount of supervillin in each cell line at 24, 48, and 72 hr by extraction with RIPA buffer [150 mM NaCl, 1% NP-40, 0.5% deoxycholic acid, 0.1% SDS, 50 mM Tris, pH 8.0, with the protease inhibitors 1 μM aprotinin,2 μM ALL-M, 1 mM benzamidine, 10 μM E64, 1 μMleupeptin, 1 μM pepstatin A, 2 mM phenylmethylsulfonyl fluoride (PMSF)]. For RNAi experiments, parental HeLa cells at 50% confluency were transfected with the Stealth dsRNAs above for 24 hrs, then lifted and plated into 6 well dishes and incubated under normal growth conditions. Samples were harvested at 48, 72, and 96 hr after transfection.

To assay the percent of bi- and multi-nucleated HeLa cells after supervillin knockdown, reverse transfections were performed using Lipofectamine RNAiMAX (Invitrogen), according to the manufacturer's instructions. Briefly, cells in DMEM-HG were plated into 6-cm dishes containing coverslips and complexed dsRNAs in OptiMEM (Invitrogen) and incubated for 69–70 hr. The coverslips were removed and fixed using paraformaldehyde (Takizawa et al. 2006). Cells remaining in the plates were extracted using RIPA buffer, as above, to confirm knockdown of supervillin. The fixed cells were stained for DNA using 1 μg/ml Hoechst, and imaged at 40x on the Zeiss Axioskop, as above. Phase and Hoechst images were compared to determine single versus multinucleated cells.

Recombinant protein purification and in vitro pull-down assays

GST-supervillin fusion proteins were purified from induced Rosetta-BL21 cells (Calbiochem, La Jolla, CA) as described previously (Chen et al. 2003; Swaffield and Johnston 2001). Briefly, cells were induced for 3 hr with 0.5 mM IPTG and collected by centrifugation. Pellets were resuspended in 15 ml lysis buffer (50 mM Tris-HCl, pH 8.0, 0.1 M NaCl, 2 mM PMSF, 1 mM EDTA, and the protease inhibitors detailed above), frozen in liquid nitrogen, and stored at −80°C. Thawed pellets were extracted by adding 20 mg/ml deoxycholic acid, 2 mM PMSF, 1 mM benzamidine, 10 μg/ml leupeptin, and 10 μg/ml antipain and sonicated for 30 sec on ice. The sonication was repeated once, and the lysates

were centrifuged in an SS-34 rotor at 12,000 rpm for 20 min. The GST-SV1009-1398 and GST–SV1398-1792 fusion proteins were then retrieved from inclusion bodies, using a protocol scaled down from that described for GST-gelsolin proteins (Puius et al. 2000). Briefly, after collection and thawing as above, the pellets were resuspended in 5 ml sucrose lysis buffer [50 mM Tris-HCl, pH 8.0, 25% sucrose (w/v), 1 mM EDTA, 0.1 mM DTT] and incubated 1 hr at room temperature with agitation. After centrifugation, the pellet was resuspended in 5 ml DOC buffer (20 mM Tris-HCl, pH 8.0, 0.2 M NaCl, 2 mM EGTA, 1% deoxycholic acid, 0.1 mM DTT), and re-centrifuged. The resulting pellet was resuspended in 5 ml Milli-Q water and re-centrifuged. The final pellet was dissolved in 5 ml urea buffer (7 M urea, 140 mM NaCl, 2.7 mM KCl, 10 mM Na_2HPO_4, 1.8 mM KH_2PO_4, 0.5 mM DTT) at 4°C overnight with rotation. After centrifugation, the supernatant was diluted to 50 ml with urea buffer and dialyzed overnight at 4°C against 500 ml (2 changes) PBS/DTT buffer (140 mM NaCl, 2.7 mM KCl, 10 mM Na_2HPO_4, 1.8 mM KH_2PO_4, 0.5 mM DTT). The dialysate was clarified by centrifugation at 44,000 x g_{avg} for 15 min at 4°C. The fusion proteins were retrieved from the supernatant by incubation with 1 ml glutathione-Sepharose 4B (GE Healthcare) for 2 hr at 4°C and transferred to a 20-ml Econo-Column (Bio-Rad Laboratories, Hercules, CA). The column was washed 5 times with 10 ml wash buffer (50 mM $NaPO_4$, pH 7.0, 300 mM NaCl, 0.05% DTT, 10% glycerol), and then 5 1-ml fractions were collected using elution buffer (wash buffer with 10 mM glutathione). Peak fractions were dialyzed in a Slide-A-Lyzer 7000 MWCO cassette (Thermo Scientific, Rockford, IL) against 500 ml of dialysis buffer (20 mM MOPS, 60 mM KCl, 0.1% DTT, 0.1 mM EGTA, and 20 μg/ml leupeptin), with two changes. The dialyzed fractions were frozen as aliquots in liquid nitrogen and stored at −80°C until use.

For GST-pull-down experiments, HeLa cells were passaged at a ratio of 1:10 onto a 10-cm tissue culture plate and grown overnight. For endogenous KIF14, the sub-confluent plate was extracted for 30 min on ice with 1 ml of modified RIPA buffer (150 mM NaCl, 1% NP-40, 0.5% deoxycholic acid, 50 mM Tris, pH 8.0, with protease inhibitors as above). Because over-expression was necessary for EPLIN extraction, HeLa cells were transfected with Flag-EPLINα using Effectene reagent, incubated overnight, and extracted as above. Cells were harvested for pull-downs by scraping, transferred to a 1.5-ml tube, sonicated for 10 sec, and centrifuged at 16,000 × g for 15 min at 4°C. The supernatant was transferred to a fresh tube, and 150 μl were added per tube to 150 μl of GST or GST-fusion protein and incubated at 4°C with rotation for 2 hr. GST-lysate mixtures were transferred to fresh 1.5-ml tubes containing 100 μl of glutathione-Sepharose 4B and incubated for 2 hr at 4°C. Beads were collected by centrifugation and washed 5 times with binding buffer (83.5 mM NaCl, 5 mM Tris, 0.025% Tween-20 pH 7.5), 1 ml per wash. Tubes were changed once during washing. Bound proteins were eluted with 300 μl of 10 mM glutathione in binding buffer, solubilized in Laemmli Sample Buffer, resolved bySDS-PAGE (Laemmli 1970), and transferred to nitrocellulose (ProtranBA85; Whatman, Dassel, Germany). Immunoblots were probed with rabbit anti-EPLIN (1:10,000), rabbit anti-KIF14 (1:1000), or goat anti-GST (1:1000) and detected using HRP-conjugated antibodies and ECL (SuperSignal WestFemto, Thermo Scientific).

RESULTS

Supervillin sequences corresponding to those in gelsolin domains G2 through G6 (Burtnick et al. 1997; Pope et al. 1998) lie mostly within structural elements responsible for the folding of these five gelsolin domains (Fig. 1). No alignment could be generated between supervillin and gelsolin repeat 1 (G1). The architecture of gelsolin repeats G2-G6 is predicted to be conserved in supervillin, with central five-stranded mixed β-sheets sandwiched between two alpha-helices. The structural similarity is apparent in repeats G2 and G3 (Fig. 1A) and pronounced for repeats G4 through G6 (Fig. 1B). In all 5 repeats, the divergent, supervillin-

specific sequences lie mostly within surface loops (Fig. 1, magenta), suggesting supervillin-specific functions and interaction partners.

To identify interactors for the supervillin C-terminus, we undertook two undirected yeast two-hybrid screens of a HeLa cell cDNA library with overlapping baits. The bait sequence encoding amino acids 834–1291 contained sequences unique to supervillin and regions of homology with gelsolin G2 and G3 repeats. The second bait encoded supervillin residues 1008–1791, which contained sequences homologous to gelsolin G2–G6 repeats and the C-terminal supervillin headpiece.

We found 33 candidate interacting sequences, representing 27 prey proteins, that passed specificity tests in subsequent directed yeast two-hybrid screens (Table 1, columns 1–4). Colonies grew faster and thus appeared earlier with the SV834-1291 bait, probably due to its smaller size (Table 1, column 5). Most prey sequences initially captured with SV834-1291 were specific for this bait, failing to cross-interact with SV1008-1791 in targeted screens (Table 1, columns 6, 7). The exception was MPHOSPH9, which was obtained as overlapping sequences [amino acids (aa) 809–858] from both screens. Nearly all the SV1008-1791 preys also interacted with SV834-1291. The exception was the most abundant prey, EPLIN/LIMA1, which was represented by two sets of clones with an overlapping sequence (EPLINβ-672–759) that emerged a total of 12 times (Table 1, column 5). These observations suggest that MPHOSPH9 aa 809–858 and most of the SV1008-1791 preys interact with sites within SV1008-1291 and that a binding site for EPLIN aa 672–759 lies within SV1291-1791.

Supervillin aa 844–864 (21-aa window) and 947–976 (28-aa window) may form coiled-coils, as predicted by the COILS program (Lupas et al. 1991). Because several of the preys obtained with SV834-1291 also contain predicted coiled-coils, we re-screened the SV834-1291 preys with bait vectors containing mutations designed to disrupt each potential supervillin coiled-coil (Table 1, columns 8, 9). The double mutation of supervillin aa Leu-952 and Leu-953 to His and Pro, respectively, did not affect any interactions (not shown). By contrast, doubly mutating supervillin Phe-851 and Leu-852 to Ser and Pro (F851S, L852P) interrupted the interactions with keratin 18, ART-27, BUB1, HAX1, lamins A/C and B2, PAN3, and TNFAIP1 in directed yeast two-hybrid screens, while interactions with the other 11 preys were maintained (Table 1, column 8). Because the prey sequences obtained for keratin 18, lamin A/C, and lamin B2 are predicted to be mostly coiled-coils, these interactions with supervillin may be incidental. However, over-expressed supervillin does mis-localize endogenous lamin A/C within the nucleus (Wulfkuhle et al. 1999). The prey sequences for ART-27, BUB1, HAX1, PAN3, and TNFAIP1 lack predicted coiled-coils, suggesting different mechanisms of association (Table 1, column 9).

To further interrogate the likelihood of specific interactions with supervillin, we embarked on classifying screens to determine which of the yeast two-hybrid prey sequences could affect supervillin function and localization in mammalian cells (Fig. 2). We first tested 23 preys plus 2 full-length cDNA constructs (ITGB3BP, RHAMM) for co-localization with EGFP-tagged SV1-1792 (EGFP-SV). Because of expected effects on assembly of the endogenous proteins (Parry et al. 2007), the coiled-coil sequences from keratin 18, lamin A/C, and lamin B were not tested. We found that 17 of the prey sequences (Table 1, asterisks) plus full-length wild-type (WT)-RHAMM co-localized with supervillin after co-expression in COS7-2 cells, supporting the existence of interactions between supervillin and these proteins (Table 1).

Hypothesizing that the short supervillin-interacting sequences might behave in a constitutively active or dominant-negative manner, we screened the co-localizing prey

constructs for effects on cell spreading (Fig. 3), a process inhibited by supervillin expression (Takizawa et al. 2007). As a sentinel for a supervillin-binding sequence with a demonstrated role in cell motility (Lai et al. 2005;Takizawa et al. 2006;Yi et al. 2002), we also included the myc-tagged TRIP6 C-terminus, aa 265–476, in all screens. We found that the TRIP6 C-terminus and four of the new candidate supervillin interactors significantly inhibited HeLa cell spreading on fibronectin (Fig. 3). The strongest effect was observed for FLNA aa 987–1186 (filamin A repeats 8–10) (Fig. 3, panel F), a sequence that contains mutations associated with human skeletal disorders (Robertson 2005;Stossel et al. 2001). Cell spreading also was decreased by transfection with BUB1 aa 4–313, MIF4GD aa 122–256, or HAX1 aa 144–279 (Fig. 3, panels B, C, D). By contrast, cell spreading was unaffected by the other prey sequences tested (Table 1), including FLNA aa 2169–2414 (repeats 20–22) (Fig. 3, panel G), which shares a conserved binding site for several ligands with FLNA repeats 8–10 (Ithychanda et al. 2009). Thus, the effect of filamin repeats 8–10 on cell spreading is probably independent of binding to the shared ligands. These results suggest effects by the TRIP6 C-terminus and four of the prey sequences on either the function of the endogenous parent protein or on its interaction with supervillin.

During the secondary screening for co-localization with EGFP-supervillin, we noticed striking shifts by many co-localizing preys on supervillin distribution, which normally includes both peripheral and internal staining (Fig. 4A, panels a–d; Fig. 4C). Of 23 co-expressed preys ($n \geq 20$ cells each), 9 increased the percentages of cells with an EGFP-supervillin concentration in the cell center from 47.7% to >65.0% (Fig. 4A–C). The prey sequence in TNFAIP1 (TNFAIP1-119-316) caused the largest shift towards the cell interior, with ~88% of the cells containing centrally located, supervillin-associated, vesicle-like structures that were lacking actin (Fig. 4A, panels e-h). HAX1-144-279, BUB1-4-313, Tks5-318-655, STARD9-2528-2663, MIF4GD-122-256, ODF2-133-269, FLNA-2169-2414, and KIF14-1522-1648) also increased the percentages of cells with a primarily central localization, as did the supervillin-binding sequence in TRIP6 (aa 265–476) (Fig. 4B–C) (Takizawa et al. 2006).

Two prey sequences shifted EGFP-supervillin towards the cell edge (Fig. 5). EPLIN-650–759 (Fig. 5A) and KIFC3-237-366 (Fig. 5B, panel b) increased the percentages of cells with a primarily peripheral supervillin signal from 1.5% in control cells to 38.1% and 31.8%, respectively (Fig. 5C). Because of difficulties in cloning the supervillin-interacting sequence in RHAMM, we also tested a dominant-negative murine RHAMM variant 4 construct (DN-RHAMM) (Fig. 5B, panel a). This construct contains mutations in 6 highly conserved charged residues outside the supervillin-interacting site in the RHAMM C-terminus. We found that DN-RHAMM caused 36.0% of the cells to have a primarily peripheral distribution of supervillin (Fig. 5C). Including this result, 12 of the new candidate supervillin-interacting sequences both co-localize with and cause mis-localization of full-length supervillin (Fig. 2).

Some of the prey sequences also affected the appearance of EGFP-supervillin (Supplementary Fig. S1). In 98% of control COS7-2 cells, supervillin appears as both linear structures associated with actin fibers and with F-actin as punctae in the cell center (Crowley et al. 2009; Wulfkuhle et al. 1999). We re-scored the cells imaged for supervillin distribution for EGFP-supervillin appearance. KIF14-1522-1648 caused the largest increase in fibrous-only appearance (to 34.8% of transfected cells *vs.* 0% of controls) (Supplementary Fig. S1A, panels e-h; Supplementary Fig. S1B), with increases in fibrous staining also observed for KIFC3-237-366 (Fig. 5B, panel b; Supplementary Fig. S1B). While Bub1-4-313 also slightly increased fibrous-only staining, it strikingly increased punctate-only staining from 0.8% in controls to 25% (Supplementary Fig. S1A, panels i-l; Supplementary Fig. S1B). Therefore, 3 out of the 12 tested prey sequences that induced mis-localization of supervillin

also caused changes in supervillin appearance; 2 of these sequences are non-motor regions of kinesins.

Many candidate supervillin interactors also caused a change in the overall cell morphology to a more rounded, unhealthy appearance (Supplementary Fig. S2). Increased expression of either TRIP6-265-476 (Supplementary Fig. S2A, panels d) or BUB1-4-313 (Supplementary Fig. S1A, panels i-l) increased cell rounding, independent of EGFP-SV (Supplementary Fig. S2C). However, expression of EGFP-SV with HAX1-144-279 or KIF14-1522-1648 increased by at least 2-fold the percent of cells that were rounded (Supplementary Fig. S2B *vs.* Supplementary Fig. S2A, panels b-c; Supplementary Fig. S2C), suggesting a synergistic effect on cell morphology.

Collectively, these results identified 12 new proteins as likely functional interactors with supervillin in mammalian cells (Table 2, column 1, bold). Eleven prey constructs and WT-RHAMM co-localized with EGFP-supervillin (Table 2, column 2). Supervillin co-localizations with sequences from EPLIN, KIF14, KIFC3, and TNFAIP1 were especially strong. Also, the BUB1-, HAX1-, STARD9-, and Tks5-interacting sites had as much signal overlap as the sequence from the demonstrated supervillin binding partner, TRIP6. The 11 prey constructs and dominant-negative RHAMM caused mis-localization of EGFP-supervillin and/or other effects, suggesting effects on supervillin interactions in vivo (Table 2, column 3). Alignments of the human prey sequences with known and predicted sequences from protein databases showed a high degree of identity across species, consistent with an evolutionarily conserved function (Table 2, column 4). The exceptions were the prey sequences from KIF14 and STARD9, which to our knowledge has not yet been cloned. While the KIF14 supervillin-interacting sequence is only 52% identical overall between human and mouse, there are several regions of high local homology that could constitute a conserved binding site. Many of the new candidate interactors regulate aspects of cell motility, membrane trafficking, ERK signaling, and extracellular matrix degradation and invasion (Table 2), similar to the established functions of supervillin (Crowley et al. 2009;Fang et al. In press;Gangopadhyay et al. 2009;Gangopadhyay et al. 2004;Takizawa et al. 2007;Takizawa et al. 2006).

We validated the predicted interactions between the supervillin C-terminus and 2 of the new candidate interactors (EPLIN, KIF14) by in vivo co-localizations of tagged full-length proteins and in vitro pull-downs with GST-supervillin fusion proteins (Fig. 6). Supervillin tagged with mRFP co-localizes almost perfectly with Flag-tagged EPLINα at intracellular punctae and apparent stress fibers (Fig. 6A, panels a–c); mRFP-supervillin also exhibits near-perfect co-localization with EGFP-tagged KIF14 at punctae (Fig. 6A, panels d–f). As expected from the selectivity shown by EPLIN for SV1008-1791 (Table 1), we recovered EPLIN from HeLa lysates with GST-tagged SV1398-1792 (Fig. 6B, lane 4) but not with GST alone or GST-SV1009-1398 (Fig. 6B, lanes 2 and 3). Similarly, as expected from the interaction of the KIF14 prey sequence with both SV834-1291 and SV1008-1791 (Table 1), endogenous KIF14 was recovered from HeLa cell lysates with GST-tagged SV1009-1398 (Fig. 6B, lane 3), but not with GST alone or GST-tagged SV1398-1792 (Fig. 6B). These results support interactions between supervillin and both KIF14 and EPLIN/LIMA1 in mammalian cells.

Because 5 of the new supervillin interactors, including EPLIN and KIF14, function during cell division (Table 2) (Carleton et al. 2006;Chircop et al. 2009;Logarinho and Bousbaa 2008;Maxwell et al. 2008;Soung et al. 2009), we explored the possibility that supervillin itself might play a role in this process (Fig. 7). To minimize potential redundancy with gelsolin (Crowley et al. 2009), we used the HeLa S3 Tet-off cells, which contain little gelsolin (not shown). We reduced the expression of supervillin using either a stably

expressed shRNA or transient treatments with dsRNAs against different supervillin sequences (Fig. 7A). All 3 supervillin-specific dsRNAs (Fig. 7B) and the shRNA increased the numbers of HeLa cells with 2 or more nuclei (Fig. 7C-D, arrows). Supervillin knockdowns with shRNA or dsRNA also increased the time required for cell doubling (Fig. 7E-F). Though all 4 reagents were effective, the largest effect was observed with a dsRNA directed against nucleotides within the supervillin 3'-UTR (Fig. 7B, 6016). These results support a role for supervillin during cell division, as predicted by the functions of its new interactors (Table 2).

To determine when supervillin functions in cell division, we imaged living, unsynchronized HeLa cells and found that supervillin-knockdown cells fail cytokinesis primarily at the stage of furrow ingression (Fig. 8; Movies M1, M2). For cells treated with a control dsRNA (Fig. 8A), the first ingression of the plasma membrane (Fig. 8A, 75′, arrow) occurred 22.0 min ± 13.9 min (mean ± s.d., n = 172) after the last frame containing an intact metaphase plate (Fig. 8A, 54′, arrowhead; Movie M1). This mean time to ingression was not significantly different from the 24.9 min ± 14.2 min (mean ± s.d., n = 187) observed for cells treated with the 6016 dsRNA (Fig. 8B–C, Movie M2). While 3.1% (6/193) of the monitored supervillin-knockdown cells *vs.* 1.6% (3/190) of the controls did not try to divide, most (84%; 36/43) of the supervillin-knockdown cells that failed cytokinesis did so after furrow initiation but before establishment of an intracellular bridge (Fig. 8B, 8D). These cells underwent multiple contractions for 55 ± 20 min (n = 12) before flattening out and migrating away as bi-nucleated cells (Fig. 8B, 180′). When supervillin-knockdown cells successfully completed cytokinesis, no significant difference was observed in the time between the initial furrow ingression and the final breakage of the cytoplasmic bridge (Fig. 8E). No more than 1% of either control or supervillin-knockdown cells underwent apoptosis during their first mitoses after 48 hr of RNAi treatment (not shown).

Consistent with a role during furrow formation, supervillin was concentrated at cleavage furrows (Fig. 9). To monitor the intracellular localization of supervillin during cell division, we stably transfected HeLa cells with EGFP-tagged human supervillin and amplified this signal in fixed cells using anti-GFP and Alexa Fluor 488-labeled secondary antibody. The total supervillin level in these cells was 3.3 ± 2.2 (means ± s.d., n = 4) times greater than endogenous supervillin levels in the parental HeLa cells (Fig. 9A). During metaphase and anaphase, supervillin was distributed throughout the cytoplasm with only a modest enrichment at the cell periphery (Fig. 9B, a–h), but became strongly concentrated at the invaginating plasma membrane during late anaphase and telophase (Fig. 9B, i–l, arrows). Supervillin also was enriched at both sides of the microtubule bundles within the intracellular bridge during cytokinesis, concentrating at the midbody (Fig. 9B, m–p, arrows) and at the presumed minus ends of the microtubule bundles at the junction between the bridge and the daughter cell cytoplasm (Fig. 9B, m–p, arrowheads).

The supervillin distribution at the membranes of dividing cells overlaps with that of its interactors, myosin IIA, EPLIN, and KIF14 (Fig. 10). During the early stages of cytokinesis, supervillin was concentrated at the cleavage furrow with myosin IIA and EPLIN (Fig. 10A, a–d; Fig. 10B, a–h; arrows). Supervillin was associated even more prominently than myosin IIA or EPLIN at the midbody (Fig. 10A, e–h; Fig. 10B, i–l; arrowheads) and overlapped at the light level with the signal for KIF14 at the midbody (Fig. 10C, a–d, arrowheads) and future abscission site (Fig. 10C, e–h, arrows), consistent with an association during cytokinesis. These localizations of supervillin and its interactors, coupled with supervillin's contribution to efficient cytokinesis, support the prediction from Table 2 that supervillin interactions play a role in cell division.

DISCUSSION

We show here that the actin-, myosin II-, and membrane-associated protein, supervillin, interacts with EPLIN and KIF14 (Fig. 6). We also identify 25 other new candidate interactors for supervillin. At least 17 of these new supervillin-binding sequences co-localize with full-length EGFP-supervillin in COS7-2 cells (Table 1). Twelve of the sequences, including those from EPLIN and KIF14, inhibit cell spreading and/or alter supervillin localization or appearance (Fig. 3–5; Table 2; Supplementary Fig. S1–S2), suggesting that these sequences disrupt supervillin's associations with endogenous proteins. For instance, the supervillin-binding site in the microtubule plus end-directed motor, KIF14 (Carleton et al. 2006;Gruneberg et al. 2006;Zhu et al. 2005), shifts EGFP-supervillin towards the cell interior (Fig. 4;Table 2), the direction expected if this fragment of KIF14 inhibits KIF14-mediated outward translocation (Fan and Beck 2004). Similarly, the interaction site in the minus end-directed motor, KIFC3 (Noda et al. 2001;Xu et al. 2002), shifts EGFP-supervillin towards the cell edge, consistent with inhibition of an inward movement (Fig. 5; Table 2). Both of these supervillin-interacting kinesin fragments reduce the appearance of supervillin in cytoplasmic "punctae" (Supplementary Fig. S1), suggesting a disruption of endosomal association.

The basis for the effect of the supervillin-binding sequence in EPLIN on interphase EGFP-supervillin distribution is less clear because this EPLIN sequence is dispensable for the F-actin binding and growth suppression activities of full-length EPLIN (Song et al. 2002). However, EPLIN co-sediments with the membrane-associated scaffold protein, septin 2 (SEPT2/Nedd5) (Chircop et al. 2009), which controls cytokinesis and myosin II interactions with kinases at stress fibers in interphase cells, as well as at the contractile ring in dividing cells (Joo et al. 2007; Kinoshita et al. 1997). Therefore, the EPLIN C-terminus may disrupt supervillin interactions with myosin II and L-MLCK at focal adhesions and stress fibers during interphase (Takizawa et al. 2006; Wulfkuhle et al. 1999).

The functions of the new supervillin interactors overlap extensively with the roles known for supervillin in cell motility, membrane trafficking, ERK signaling, and extracellular matrix invasion (Table 2) (Crowley et al. 2009;Fang et al. In press;Gangopadhyay et al. 2009;Gangopadhyay et al. 2004;Takizawa et al. 2007;Takizawa et al. 2006). A further role for supervillin in cell division is predicted by the cellular phenotypes of 5 of the new interactors (BUB1, EPLIN, KIF14, ODF2/Cenexin, and RHAMM) (Carleton et al. 2006;Chircop et al. 2009;Logarinho and Bousbaa 2008;Maxwell et al. 2008;Soung et al. 2009). In addition, the supervillin N-terminus binds to the myosin II heavy chain, L-MLCK, F-actin, and cortactin (Fig. 11) (Chen et al. 2003;Crowley et al. 2009;Pestonjamasp et al. 1995;Takizawa et al. 2007), all of which are involved in mitosis or cytokinesis (Kunda and Baum 2009;Matsumura 2005;Ng et al. 2005;Wang et al. 2008). Thus, the biochemical signature of supervillin-associated proteins suggests a function for supervillin during cell division.

As predicted, supervillin does contribute to the establishment or maintenance of the cytokinetic furrow. Because furrow formation is not significantly delayed in cells with reduced levels of supervillin (Fig. 8C), spindle assembly apparently occurs with normal kinetics. Instead, supervillin-knockdown cells fail division during early cytokinesis (Fig. 7–8), and supervillin overlaps with myosin IIA and EPLIN at the cleavage furrow and with KIF14 at the midbody (Fig. 9–10). The incomplete penetrance of the supervillin-knockdown phenotype may be due to variable amounts of residual supervillin at the time of cleavage or to functional redundancy with other gelsolin family members, although gelsolin itself is virtually absent in these HeLa cells. A role for supervillin during cell division therefore

provides functional validation for the constellation of new interactors identified here (Table 2).

Supervillin's function at the cleavage furrow may be the coordination of L-MLCK-mediated myosin II activation with the attachment of the contractile apparatus to the membrane through EPLIN and SEPT2. Supervillin promotes myosin II activation by L-MLCK and binds directly to both proteins (Fig. 11) (Takizawa et al. 2007). L-MLCK concentrates at the cleavage furrow; and MLCK inhibitors and the over-expression of the supervillin-binding N-terminus of L-MLCK both cause cytokinesis failure (Dulyaninova et al. 2004;Lucero et al. 2006;Poperechnaya et al. 2000;Wong et al. 2007). However, multiple contractions apparently occur in supervillin-knockdown cells before cleavage fails (Fig. 8), implying that myosin II is appropriately activated. Assuming that supervillin can bind simultaneously to myosin II and EPLIN, which also is required for normal cytokinesis (Chircop et al. 2009), supervillin could bridge myosin II/L-MLCK with septins at the plasma membrane through EPLIN (Fig. 6) or other membrane interactors (Nebl et al. 2002;Pestonjamasp et al. 1997;Takizawa et al. 2006). Such a supervillin-based scaffold could work in parallel with scaffolds associated with anillin, another actin-, myosin II-, and membrane-binding protein required for early cytokinesis (Piekny and Glotzer 2008;von Dassow 2009).

A supervillin scaffold also might help localize KIF14 and other central spindle proteins to the vicinity of the membrane during the formation of the intracellular bridge. KIF14-knockdown cells either fail to initiate mitosis or cannot cleave at the midbody in late cytokinesis, depending on the extent of the knockdown (Carleton et al. 2006; Zhu et al. 2005). Supervillin-knockdown cells fail earlier, before the formation of an intracellular bridge and midbody (Fig. 8B), suggesting that the supervillin-KIF14 interaction may be important prior to KIF14 function at the midbody. For instance, supervillin's 3 binding sites for F-actin (Chen et al. 2003) may contribute to the actin-dependent contact between the furrow membrane and the spindle mid-zone that is proposed to regulate the site of cleavage (Martineau et al. 1995). Potential supervillin-binding partners in the spindle also include the kinesin KIF4A (Kurasawa et al. 2004; Takizawa et al. 2006; Zhu and Jiang 2005), as well as KIF14. In interphase cells, the supervillin-interacting sequence within KIF4A mis-localizes EGFP-supervillin towards the cell interior without a strong co-localization (not shown). The association of supervillin with non-motor domains of at least 3 kinesin family proteins (KIF14, KIFC3, STARD9) suggests a general role for supervillin and associated proteins in coordinating microtubule motors with actin and myosin II functions at membranes.

Such a general role might include the transport of cytoskeletal or signaling proteins to the furrow by supervillin and its binding partners. Trafficking to the cleavage furrow of Src family kinases, 'lipid raft' membranes, and Arf6- and Rab11-associated recycling endosomes is required for early steps in cytokinesis (Joo et al. 2005; Kasahara et al. 2007; Montagnac et al. 2008; Ng et al. 2005; Prekeris and Gould 2008). Supervillin co-fractionates with lipid rafts, promotes the rapid recycling of integrins in peripheral endosomes, and associates with punctae that contain the Src-activating GTPase RhoB and exhibit kinesin-like movements in interphase cells (Crowley et al. 2009; Fang et al. In press; Nebl et al. 2002). ERK activation by supervillin isoforms also could contribute to both early and late steps in cytokinesis (Fang et al. In press; Gangopadhyay et al. 2009; Gangopadhyay et al. 2004; Kasahara et al. 2007). Thus, the interactions with the kinesins implicated in this study could be crucial for the trafficking of endosomes and signaling proteins to the assembling furrow, as well as for furrow stability.

The large percentage of supervillin interactors implicated in carcinogenesis (Table 2) and the roles documented for other supervillin family members during cell migration, matrix invasion, and cytoskeletal and transcriptional regulation are consistent with functions in cell

proliferation and tumor progression (Archer et al. 2005;Khurana and George 2008;Van den Abbeele et al. 2007). Supervillin itself is implicated as a predisposing factor in non-BRCA1/2 breast cancer (Hedenfalk et al. 2003;Vanaja et al. 2006). The new supervillin interactors reported here support a role for supervillin as a scaffold and coordinator of membranes and motors during motile processes and suggest that biochemical and functional cross-talk among this group of proteins may reveal novel molecular mechanisms associated with tumorigenesis.

Supplementary Material

Refer to Web version on PubMed Central for supplementary material.

Acknowledgments

We thank Mr. Joshua Nordberg for help with the multimode microscope and Drs. Greenfield Sluder and Craig Ceol for helpful discussions and comments on the manuscript. We also thank Drs. Michael Carleton, Mark Ginsberg, R. Scott Maul, and Eva Turley for gifts of plasmids and antibodies. In addition, we gratefully acknowledge Dr. Norio Takizawa for screening cell lines for gelsolin expression, Gloried Ebsworth for assistance with primer design, and Drs. Dannel McCollum, Mary Munson, and Yumi Uetake for their advice on aspects of this project. This project was supported by NIH grant GM033048 to E.J.L. and benefited from NIH Biomedical Instrumentation Grant #1S1ORR015775 to Dr. Greenfield Sluder for the shared multimode microscope used in live cell imaging.

References

Akhmanova A, Stehbens SJ, Yap AS. Touch, grasp, deliver and control: functional cross-talk between microtubules and cell adhesions. Traffic. 2009; 10:268–74. [PubMed: 19175539]

Archer SK, Claudianos C, Campbell HD. Evolution of the gelsolin family of actin-binding proteins as novel transcriptional coactivators. Bioessays. 2005; 27:388–96. [PubMed: 15770676]

Arnold K, Bordoli L, Kopp J, Schwede T. The SWISS-MODEL workspace: a web-based environment for protein structure homology modelling. Bioinformatics. 2006; 22:195–201. [PubMed: 16301204]

Brown JW, Vardar-Ulu D, McKnight CJ. How to arm a supervillin: Designing F-actin binding activity into supervillin headpiece. J Mol Biol. 2009; 393:608–18. [PubMed: 19683541]

Burtnick LD, Koepf EK, Grimes J, Jones EY, Stuart DI, McLaughlin PJ, Robinson RC. The crystal structure of plasma gelsolin: implications for actin severing, capping, and nucleation. Cell. 1997; 90:661–70. [PubMed: 9288746]

Carleton M, Mao M, Biery M, Warrener P, Kim S, Buser C, Marshall CG, Fernandes C, Annis J, Linsley PS. RNA interference-mediated silencing of mitotic kinesin KIF14 disrupts cell cycle progression and induces cytokinesis failure. Mol Cell Biol. 2006; 26:3853–63. [PubMed: 16648480]

Caviston JP, Holzbaur EL. Microtubule motors at the intersection of trafficking and transport. Trends Cell Biol. 2006; 16:530–7. [PubMed: 16938456]

Chan W, Calderon G, Swift AL, Moseley J, Li S, Hosoya H, Arias IM, Ortiz DF. Myosin II regulatory light chain is required for trafficking of bile salt export protein to the apical membrane in Madin-Darby canine kidney cells. J Biol Chem. 2005; 280:23741–7. [PubMed: 15826951]

Chen Y, Takizawa N, Crowley JL, Oh SW, Gatto CL, Kambara T, Sato O, Li X, Ikebe M, Luna EJ. F-actin and myosin II binding domains in supervillin. J Biol Chem. 2003; 278:46094–46106. [PubMed: 12917436]

Chircop M, Oakes V, Graham ME, Ma MP, Smith CM, Robinson PJ, Khanna KK. The actin-binding and bundling protein, EPLIN, is required for cytokinesis. Cell Cycle. 2009; 8:757–64. [PubMed: 19221476]

Chumnarnsilpa S, Loonchanta A, Xue B, Choe H, Urosev D, Wang H, Lindberg U, Burtnick LD, Robinson RC. Calcium ion exchange in crystalline gelsolin. J Mol Biol. 2006; 357:773–82. [PubMed: 16466744]

Claudianos C, Campbell HD. The novel flightless-I gene brings together two gene families, actin-binding proteins related to gelsolin and leucine-rich-repeat proteins involved in Ras signal transduction. Mol Biol Evol. 1995; 12:405–14. [PubMed: 7739382]

Crowley JL, Smith TC, Fang Z, Takizawa N, Luna EJ. Supervillin reorganizes the actin cytoskeleton and increases invadopodial efficiency. Mol Biol Cell. 2009; 20:948–62. [PubMed: 19109420]

Dulyaninova NG, Patskovsky YV, Bresnick AR. The N-terminus of the long MLCK induces a disruption in normal spindle morphology and metaphase arrest. J Cell Sci. 2004; 117:1481–93. [PubMed: 15020676]

Even-Ram S, Doyle AD, Conti MA, Matsumoto K, Adelstein RS, Yamada KM. Myosin IIA regulates cell motility and actomyosin-microtubule crosstalk. Nat Cell Biol. 2007; 9:299–309. [PubMed: 17310241]

Fan J, Beck KA. A role for the spectrin superfamily member Syne-1 and kinesin II in cytokinesis. J Cell Sci. 2004; 117:619–29. [PubMed: 14709720]

Fang Z, Takizawa N, Wilson KA, Smith TC, Delprato A, Davidson MW, Lambright DG, Luna EJ. The membrane-associated protein, supervillin, accelerates rapid integrin recycling and cell motility. Traffic. In press.

Gangopadhyay SS, Kengni E, Appel S, Gallant C, Kim HR, Leavis P, DeGnore J, Morgan KG. Smooth muscle archvillin is an ERK scaffolding protein. J Biol Chem. 2009; 284:17607–15. [PubMed: 19406750]

Gangopadhyay SS, Takizawa N, Gallant C, Barber AL, Je HD, Smith TC, Luna EJ, Morgan KG. Smooth muscle archvillin: A novel regulator of signaling and contractility in vascular smooth muscle. J Cell Sci. 2004; 117:5043–57. [PubMed: 15383618]

Gimona M, Buccione R, Courtneidge SA, Linder S. Assembly and biological role of podosomes and invadopodia. Curr Opin Cell Biol. 2008; 20:235–41. [PubMed: 18337078]

Glotzer M. The molecular requirements for cytokinesis. Science. 2005; 307:1735–9. [PubMed: 15774750]

Gruneberg U, Neef R, Li X, Chan EH, Chalamalasetty RB, Nigg EA, Barr FA. KIF14 and citron kinase act together to promote efficient cytokinesis. J Cell Biol. 2006; 172:363–72. [PubMed: 16431929]

Hall CL, Turley EA. Hyaluronan: RHAMM mediated cell locomotion and signaling in tumorigenesis. J Neurooncol. 1995; 26:221–9. [PubMed: 8750188]

Harper JV. Synchronization of cell populations in G1/S and G2/M phases of the cell cycle. Methods Mol Biol. 2005; 296:157–66. [PubMed: 15576930]

Hedenfalk I, Ringner M, Ben-Dor A, Yakhini Z, Chen Y, Chebil G, Ach R, Loman N, Olsson H, Meltzer P, et al. Molecular classification of familial non-BRCA1/BRCA2 breast cancer. Proc Natl Acad Sci U S A. 2003; 100(5):2532–7. [PubMed: 12610208]

Hickson GR, O'Farrell PH. Anillin: a pivotal organizer of the cytokinetic machinery. Biochem Soc Trans. 2008; 36:439–41. [PubMed: 18481976]

Hirokawa N, Noda Y. Intracellular transport and kinesin superfamily proteins, KIFs: structure, function, and dynamics. Physiol Rev. 2008; 88:1089–118. [PubMed: 18626067]

Ithychanda SS, Hsu D, Li H, Yan L, Liu D, Das M, Plow EF, Qin J. Identification and characterization of multiple similar ligand-binding repeats in filamin: implication on filamin-mediated receptor clustering and cross-talk. J Biol Chem. 2009; 284(50):35113–21. [PubMed: 19828450]

Joo E, Surka MC, Trimble WS. Mammalian SEPT2 is required for scaffolding nonmuscle myosin II and its kinases. Dev Cell. 2007; 13:677–90. [PubMed: 17981136]

Joo E, Tsang CW, Trimble WS. Septins: traffic control at the cytokinesis intersection. Traffic. 2005; 6:626–34. [PubMed: 15998319]

Kasahara K, Nakayama Y, Nakazato Y, Ikeda K, Kuga T, Yamaguchi N. Src signaling regulates completion of abscission in cytokinesis through ERK/MAPK activation at the midbody. J Biol Chem. 2007; 282:5327–39. [PubMed: 17189253]

Khurana S, George SP. Regulation of cell structure and function by actin-binding proteins: Villin's perspective. FEBS Lett. 2008; 582:2128–39. [PubMed: 18307996]

Kinoshita M, Kumar S, Mizoguchi A, Ide C, Kinoshita A, Haraguchi T, Hiraoka Y, Noda M. Nedd5, a mammalian septin, is a novel cytoskeletal component interacting with actin-based structures. Genes Dev. 1997; 11:1535–47. [PubMed: 9203580]

Kunda P, Baum B. The actin cytoskeleton in spindle assembly and positioning. Trends Cell Biol. 2009; 19:174–9. [PubMed: 19285869]

Kurasawa Y, Earnshaw WC, Mochizuki Y, Dohmae N, Todokoro K. Essential roles of KIF4 and its binding partner PRC1 in organized central spindle midzone formation. EMBO J. 2004; 23:3237–48. [PubMed: 15297875]

Laemmli UK. Cleavage of structural proteins during the assembly of the head of bacteriophage T4. Nature (Lond). 1970; 227:680–685. [PubMed: 5432063]

Lai YJ, Chen CS, Lin WC, Lin FT. c-Src-mediated phosphorylation of TRIP6 regulates its function in lysophosphatidic acid-induced cell migration. Mol Cell Biol. 2005; 25:5859–68. [PubMed: 15988003]

Logarinho E, Bousbaa H. Kinetochore-microtubule interactions “in check” by Bub1, Bub3 and BubR1: The dual task of attaching and signalling. Cell Cycle. 2008; 7:1763–8. [PubMed: 18594200]

Lucero A, Stack C, Bresnick AR, Shuster CB. A global, myosin light chain kinase-dependent increase in myosin II contractility accompanies the metaphase-anaphase transition in sea urchin eggs. Mol Biol Cell. 2006; 17:4093–104. [PubMed: 16837551]

Lupas A, Van Dyke M, Stock J. Predicting coiled coils from protein sequences. Science. 1991; 252:1162–4.

Martineau SN, Andreassen PR, Margolis RL. Delay of HeLa cell cleavage into interphase using dihydrocytochalasin B: retention of a postmitotic spindle and telophase disc correlates with synchronous cleavage recovery. J Cell Biol. 1995; 131:191–205. [PubMed: 7559776]

Matsumura F. Regulation of myosin II during cytokinesis in higher eukaryotes. Trends Cell Biol. 2005; 15:371–7. [PubMed: 15935670]

Maxwell CA, McCarthy J, Turley E. Cell-surface and mitotic-spindle RHAMM: moonlighting or dual oncogenic functions? J Cell Sci. 2008; 121:925–32. [PubMed: 18354082]

Montagnac G, Echard A, Chavrier P. Endocytic traffic in animal cell cytokinesis. Curr Opin Cell Biol. 2008; 20:454–61. [PubMed: 18472411]

Nebl T, Pestonjamasp KN, Leszyk JD, Crowley JL, Oh SW, Luna EJ. Proteomic analysis of a detergent-resistant membrane skeleton from neutrophil plasma membranes. J Biol Chem. 2002; 277:43399–409. [PubMed: 12202484]

Ng MM, Chang F, Burgess DR. Movement of membrane domains and requirement of membrane signaling molecules for cytokinesis. Dev Cell. 2005; 9:781–90. [PubMed: 16326390]

Noda Y, Okada Y, Saito N, Setou M, Xu Y, Zhang Z, Hirokawa N. KIFC3, a microtubule minus end-directed motor for the apical transport of annexin XIIIb-associated Triton-insoluble membranes. J Cell Biol. 2001; 155:77–88. [PubMed: 11581287]

Oh SW, Pope RK, Smith KP, Crowley JL, Nebl T, Lawrence JB, Luna EJ. Archvillin, a muscle-specific isoform of supervillin, is an early expressed component of the costameric membrane skeleton. J Cell Sci. 2003; 116:2261–2275. [PubMed: 12711699]

Parry DA, Strelkov SV, Burkhard P, Aebi U, Herrmann H. Towards a molecular description of intermediate filament structure and assembly. Exp Cell Res. 2007; 313:2204–16. [PubMed: 17521629]

Pestonjamasp K, Amieva MR, Strassel CP, Nauseef WM, Furthmayr H, Luna EJ. Moesin, ezrin, and p205 are actin-binding proteins associated with neutrophil plasma membranes. Mol Biol Cell. 1995; 6:247–259. [PubMed: 7612961]

Pestonjamasp KN, Pope RK, Wulfkuhle JD, Luna EJ. Supervillin (p205): A novel membrane-associated, F-actin-binding protein in the villin/gelsolin superfamily. J Cell Biol. 1997; 139:1255–69. [PubMed: 9382871]

Piekny AJ, Glotzer M. Anillin is a scaffold protein that links RhoA, actin, and myosin during cytokinesis. Curr Biol. 2008; 18:30–6. [PubMed: 18158243]

Pope RK, Pestonjamasp KN, Smith KP, Wulfkuhle JD, Strassel CP, Lawrence JB, Luna EJ. Cloning, characterization, and chromosomal localization of human supervillin (SVIL). Genomics. 1998; 52:342–51. [PubMed: 9867483]

Poperechnaya A, Varlamova O, Lin PJ, Stull JT, Bresnick AR. Localization and activity of myosin light chain kinase isoforms during the cell cycle. J Cell Biol. 2000; 151:697–708. [PubMed: 11062269]

Prekeris R, Gould GW. Breaking up is hard to do - membrane traffic in cytokinesis. J Cell Sci. 2008; 121:1569–76. [PubMed: 18469013]

Puius YA, Fedorov EV, Eichinger L, Schleicher M, Almo SC. Mapping the functional surface of domain 2 in the gelsolin superfamily. Biochemistry. 2000; 39:5322–31. [PubMed: 10820002]

Robertson SP. Filamin A: phenotypic diversity. Curr Opin Genet Dev. 2005; 15:301–7. [PubMed: 15917206]

Robinson RC, Mejillano M, Le VP, Burtnick LD, Yin HL, Choe S. Domain movement in gelsolin: a calcium-activated switch. Science. 1999; 286:1939–42. [PubMed: 10583954]

Shattil SJ, O'Toole T, Eigenthaler M, Thon V, Williams M, Babior BM, Ginsberg MH. b_3-endonexin, a novel polypeptide that interacts specifically with the cytoplasmic tail of the integrin b_3 subunit. J Cell Biol. 1995; 131:807–816. [PubMed: 7593198]

Soldati T, Schliwa M. Powering membrane traffic in endocytosis and recycling. Nat Rev Mol Cell Biol. 2006; 7:897–908. [PubMed: 17139330]

Song Y, Maul RS, Gerbin CS, Chang DD. Inhibition of anchorage-independent growth of transformed NIH3T3 cells by epithelial protein lost in neoplasm (EPLIN) requires localization of EPLIN to actin cytoskeleton. Mol Biol Cell. 2002; 13:1408–16. [PubMed: 11950948]

Soung NK, Park JE, Yu LR, Lee KH, Lee JM, Bang JK, Veenstra TD, Rhee K, Lee KS. Plk1-dependent and -independent roles of an ODF2 splice variant, hCenexin1, at the centrosome of somatic cells. Dev Cell. 2009; 16:539–50. [PubMed: 19386263]

Stossel TP, Condeelis J, Cooley L, Hartwig JH, Noegel A, Schleicher M, Shapiro SS. Filamins as integrators of cell mechanics and signalling. Nat Rev Mol Cell Biol. 2001; 2:138–45. [PubMed: 11252955]

Swaffield JC, Johnston SA. Affinity purification of proteins binding to GST fusion proteins. Curr Protoc Mol Biol. 2001; Chapter 20(Unit 20.2)

Takizawa N, Ikebe R, Ikebe M, Luna EJ. Supervillin slows cell spreading by facilitating myosin II activation at the cell periphery. J Cell Sci. 2007; 120:3792–803. [PubMed: 17925381]

Takizawa N, Smith TC, Nebl T, Crowley JL, Palmieri SJ, Lifshitz LM, Ehrhardt AG, Hoffman LM, Beckerle MC, Luna EJ. Supervillin modulation of focal adhesions involving TRIP6/ZRP-1. J Cell Biol. 2006; 174:447–58. [PubMed: 16880273]

Ting HJ, Yeh S, Nishimura K, Chang C. Supervillin associates with androgen receptor and modulates its transcriptional activity. Proc Natl Acad Sci U S A. 2002; 99:661–6. [PubMed: 11792840]

Urosev D, Ma Q, Tan AL, Robinson RC, Burtnick LD. The structure of gelsolin bound to ATP. J Mol Biol. 2006; 357:765–72. [PubMed: 16469333]

Van den Abbeele A, De Corte V, Van Impe K, Bruyneel E, Boucherie C, Bracke M, Vandekerckhove J, Gettemans J. Downregulation of gelsolin family proteins counteracts cancer cell invasion in vitro. Cancer Lett. 2007; 255:57–70. [PubMed: 17493746]

Vanaja DK, Ballman KV, Morlan BW, Cheville JC, Neumann RM, Lieber MM, Tindall DJ, Young CY. PDLIM4 repression by hypermethylation as a potential biomarker for prostate cancer. Clin Cancer Res. 2006; 12:1128–36. [PubMed: 16489065]

Vardar D, Chishti AH, Frank BS, Luna EJ, Noegel AA, Oh SW, Schleicher M, McKnight CJ. Villin-type headpiece domains show a wide range of F-actin-binding affinities. Cell Motil Cytoskeleton. 2002; 52:9–21. [PubMed: 11977079]

Vascotto F, Lankar D, Faure-Andre G, Vargas P, Diaz J, Le Roux D, Yuseff MI, Sibarita JB, Boes M, Raposo G, et al. The actin-based motor protein myosin II regulates MHC class II trafficking and BCR-driven antigen presentation. J Cell Biol. 2007; 176:1007–19. [PubMed: 17389233]

Vicente-Manzanares M, Zareno J, Whitmore L, Choi CK, Horwitz AF. Regulation of protrusion, adhesion dynamics, and polarity by myosins IIA and IIB in migrating cells. J Cell Biol. 2007; 176:573–80. [PubMed: 17312025]

von Dassow G. Concurrent cues for cytokinetic furrow induction in animal cells. Trends Cell Biol. 2009; 19:165–73. [PubMed: 19285868]

Wang W, Chen L, Ding Y, Jin J, Liao K. Centrosome separation driven by actin-microfilaments during mitosis is mediated by centrosome-associated tyrosine-phosphorylated cortactin. J Cell Sci. 2008; 121:1334–43. [PubMed: 18388321]

Wong R, Fabian L, Forer A, Brill JA. Phospholipase C and myosin light chain kinase inhibition define a common step in actin regulation during cytokinesis. BMC Cell Biol. 2007; 8:15. [PubMed: 17509155]

Wulfkuhle JD, Donina IE, Stark NH, Pope RK, Pestonjamasp KN, Niswonger ML, Luna EJ. Domain analysis of supervillin, an F-actin bundling plasma membrane protein with functional nuclear localization signals. J Cell Sci. 1999; 112:2125–36. [PubMed: 10362542]

Xu Y, Takeda S, Nakata T, Noda Y, Tanaka Y, Hirokawa N. Role of KIFC3 motor protein in Golgi positioning and integration. J Cell Biol. 2002; 158:293–303. [PubMed: 12135985]

Yi J, Kloeker S, Jensen CC, Bockholt S, Honda H, Hirai H, Beckerle MC. Members of the Zyxin family of LIM proteins interact with members of the p130Cas family of signal transducers. J Biol Chem. 2002; 277:9580–9. [PubMed: 11782456]

Zhu C, Jiang W. Cell cycle-dependent translocation of PRC1 on the spindle by Kif4 is essential for midzone formation and cytokinesis. Proc Natl Acad Sci U S A. 2005; 102:343–8. [PubMed: 15625105]

Zhu C, Zhao J, Bibikova M, Leverson JD, Bossy-Wetzel E, Fan JB, Abraham RT, Jiang W. Functional analysis of human microtubule-based motor proteins, the kinesins and dyneins, in mitosis/cytokinesis using RNA interference. Mol Biol Cell. 2005; 16:3187–99. [PubMed: 15843429]

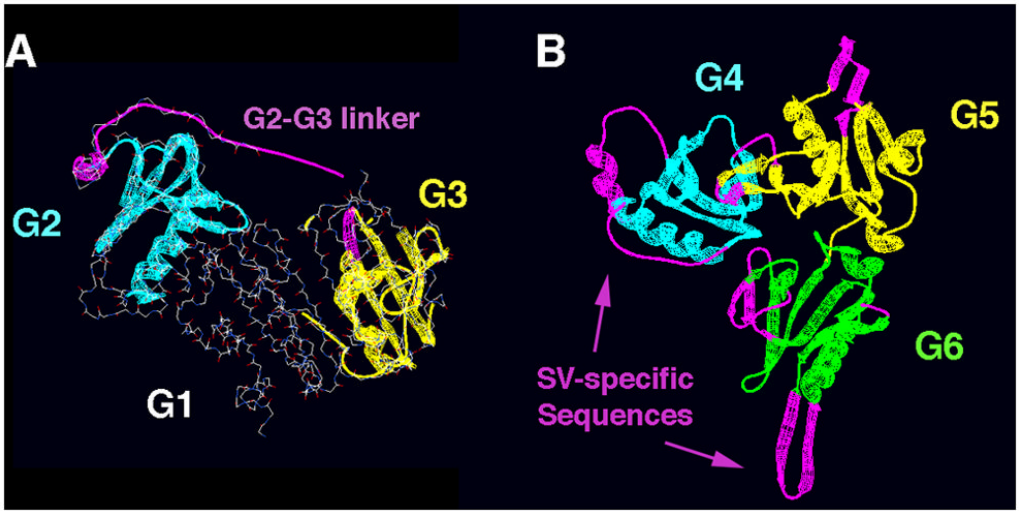

Fig. 1.

Structural models of (**A**) supervillin amino acids 1019–1306 based on gelsolin repeats G2–G3 (residues 189–444) and (**B**) supervillin amino acids 1326–1699 based on gelsolin repeats G4–G6 (residues 445–765). Supervillin-specific sequences (**magenta**) predominate at external loops, which contain amino acid insertions and deletions, as compared with the corresponding loop sequences in gelsolin. **Panel A**, the gelsolin sequence in wire frame mode is superimposed over the supervillin sequence shown as a ribbon to denote the location of gelsolin repeat G1, which is dissimilar. Supervillin sequences modeled on gelsolin repeats 2 (**G2**) and 3 (**G3**) are shown in cyan and yellow, respectively. **Panel B**, only the supervillin ribbon sequence is shown. Supervillin repeats similar to gelsolin repeats 4 (**G4**) 5 (**G5**), and 6 (**G6**) are shown in cyan, yellow, and green, respectively. Locations of supervillin-specific regions are shown in magenta.

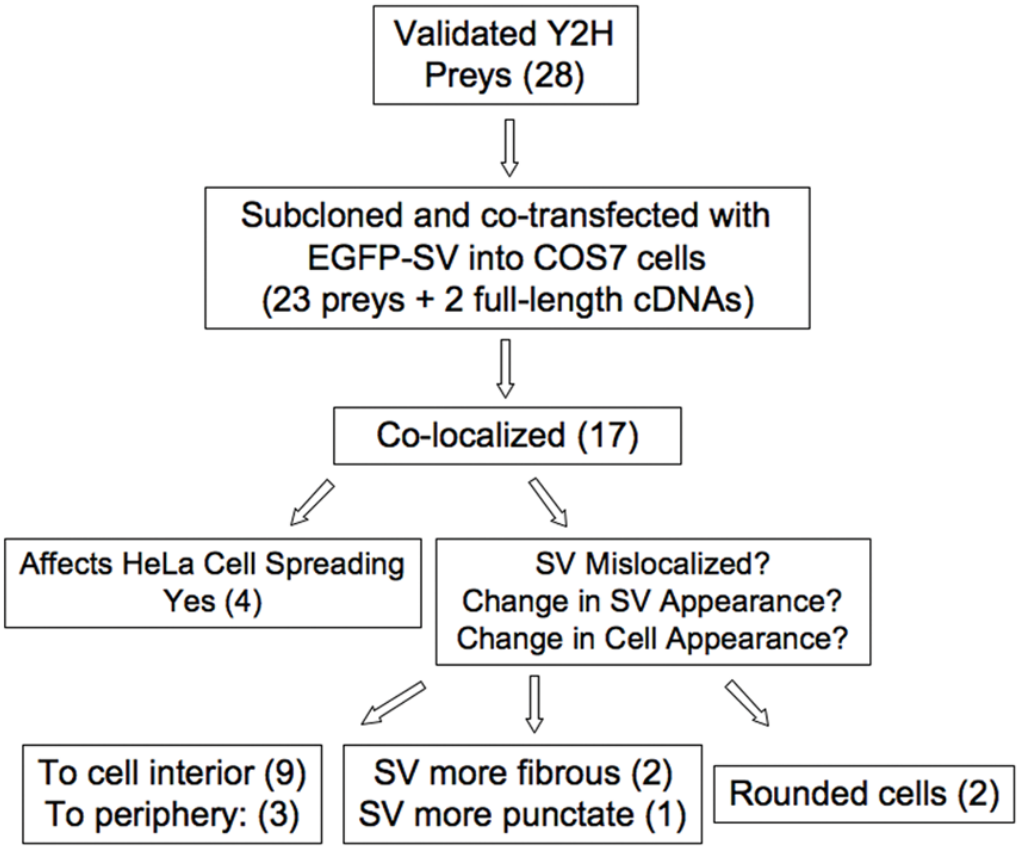

Fig. 2.

Flow chart for screening of supervillin-interacting sequences in mammalian cells. Prey sequences were cloned into mammalian expression vectors and screened for effects on HeLa cell spreading onto fibronectin, for changes to COS7-2 cell morphology, and for effects on the appearance and localization of supervillin as described in the text. Twelve prey sequences emerged from these screens as new candidate supervillin-binding proteins.

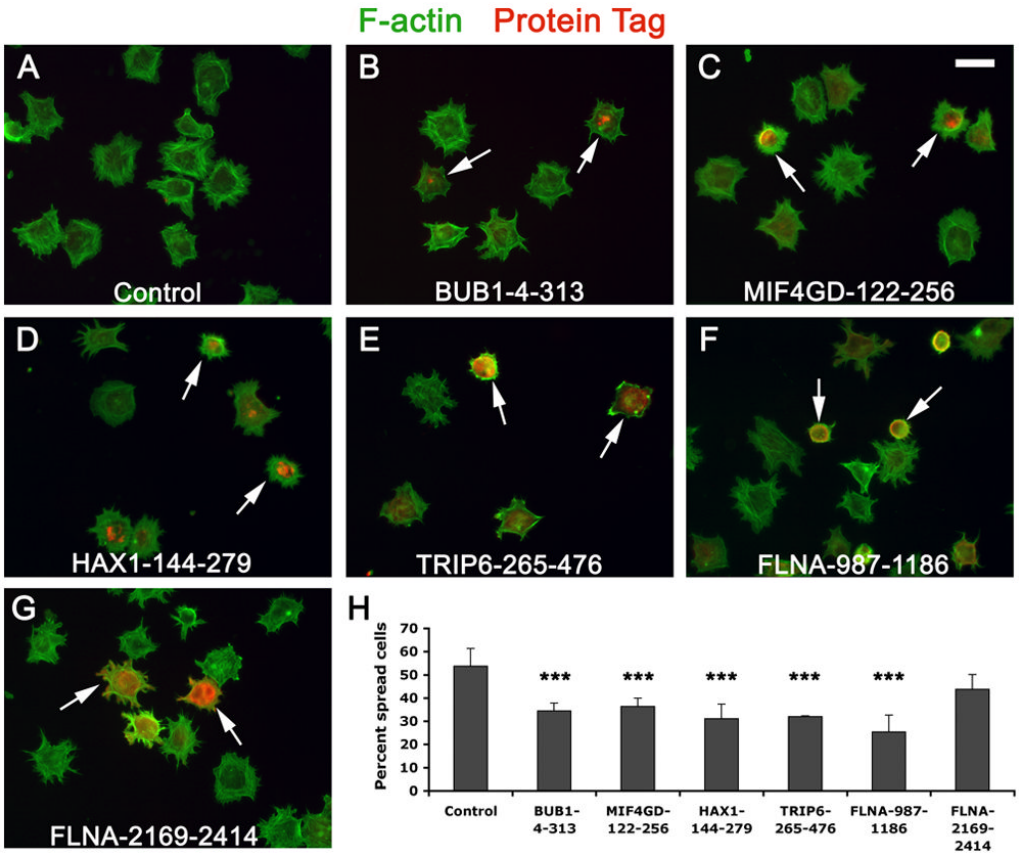

Fig. 3.

Prey constructs with effects on the initial spreading of HeLa cells on fibronectin. Transfected HeLa cells expressing a tagged control pCMV vector (**A**) or this vector with sequences encoding (**B**) BUB1(4–313), (**C**) MIF4GD(122–256), (**D**) HAX1(144–279), (**E**) TRIP6(265–476) as a sentinel, (**F**) FLNA(987–1186) or (**G**) FLNA(2169–2414) were fixed after spreading for 30 min onto fibronectin, stained for F-actin (green) and protein tag (red) and scored for spreading (Takizawa et al. 2007). BUB1(4–313), MIF4GD(122–256), HAX1(144–279), TRIP6(265–476), and FLNA(987–1186) all significantly inhibited cell spreading, but FLNA(2169–2414) had no effect. (**A**–**G**) Size bar = 25 μm; arrows indicate cells expressing tagged prey constructs. (**H**) Graph showing the percentage of spread cells after 30 min on fibronectin. Means ± s.d. from a total of 6 coverslips from 2 experiments, 30 fields (75 to >200 cells) per coverslip; ***, $p < 0.001$ using ANOVA.

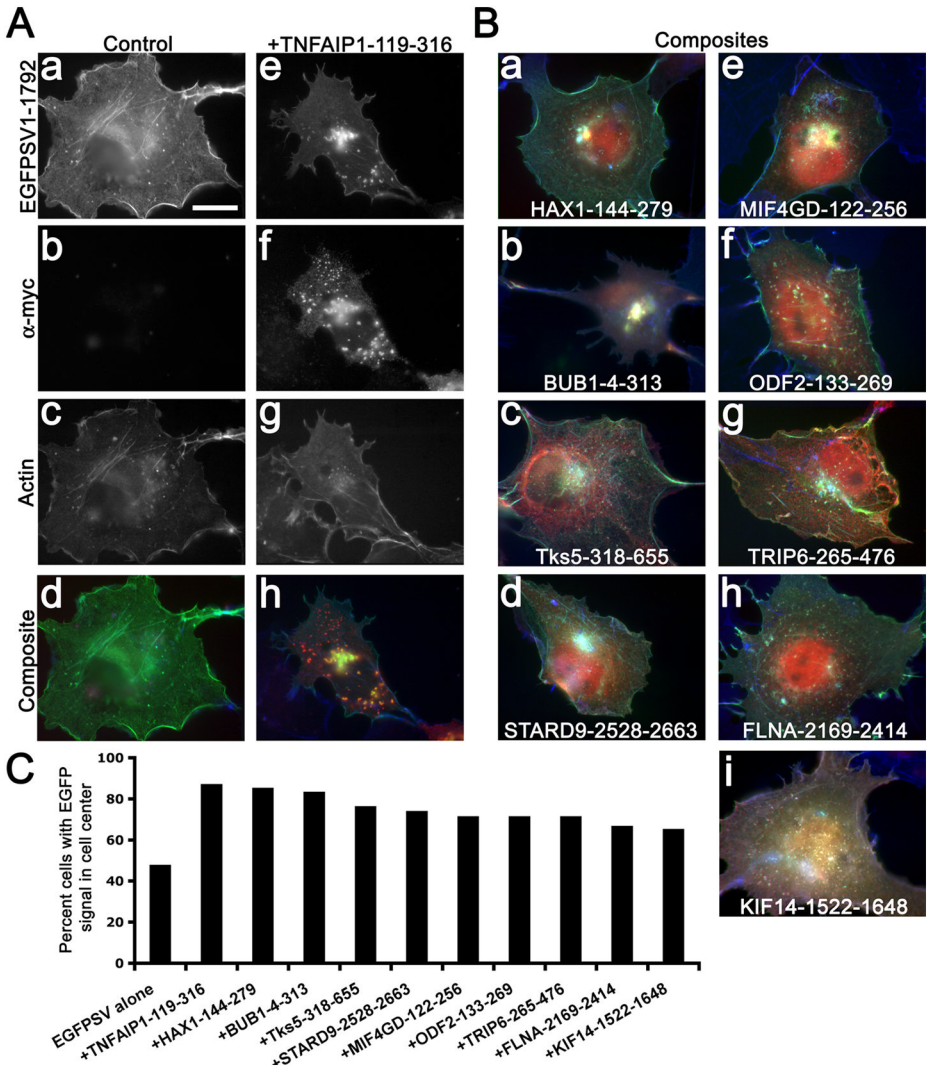

Fig. 4.

Prey constructs altering the amount of internal EGFP-supervillin signal. (**A**) COS7-2 cells expressing control myc vector (**a–d**) or myc-tagged TNFAIP1(119–316) (**e–h**) were imaged for EGFP-supervillin (**a, e**), myc-staining (**b, f**), and F-actin (**c, g**); images were pseudo-colored green, red, and blue, respectively, in the composite images (**d, h**). (**B**) Similarly generated composite images for COS7-2 cells co-expressing EGFP-supervillin and (**a**) HAX1(144–279), (**b**) BUB1(4–313), (**c**) Tks5(318–655), (**d**) STARD9(2528–2663), (**e**) MIF4GD(122–256) (**f**) ODF2(133–269), (**g**) TRIP6(265–476) positive control, (**h**) FLNA(2169–2414), and (i) KIF14(1522–1648). (**A, B**) Bar, 20 μm. (**C**) Graph showing the percentage of cells with altered cytoplasmic staining (n >20).

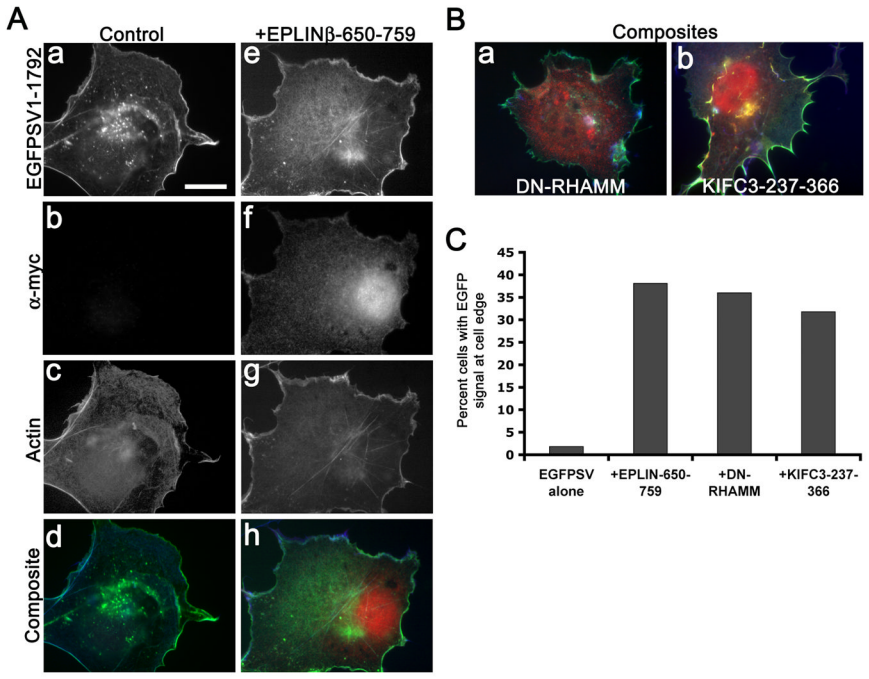

Fig. 5.

Prey constructs targeting EGFP-supervillin to the cell edge. (**A**) COS7-2 cells expressing control myc vector (**a–d**) or myc-tagged EPLIN(650–759) (**e**–**h**) were imaged for EGFP-supervillin (**a, e**), myc-staining (**b, f**), and F-actin (**c, g**); images were pseudo-colored green, red, and blue, respectively, in composite images (**d, h**). (**B**) Similarly generated composite images for COS7-2 cells co-expressing EGFP-supervillin and (**a**) dominant-negative (DN) RHAMM or (**b**) KIFC3(237–366). (**A, B**) Bar, 20 μm. (**C**) Graph showing the percentage of cells with predominant staining at the cell edge (n >20).

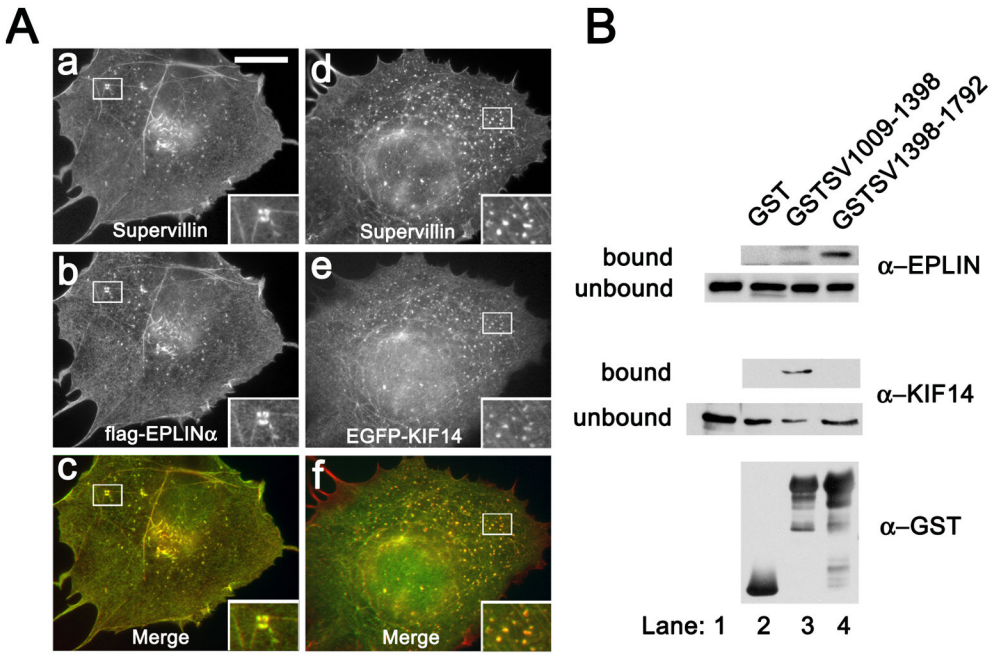

Fig. 6.

Co-localization and binding of SV with EPLIN and KIF14. (**A**) Co-expressed mRFP-SV (**a, d; red in c, f**) co-localizes almost perfectly with Flag-EPLINα (**b; green in c**) and with EGFP-KIF14 (**e; green in f**) in COS7-2 cells; overlaps appear yellow (**c, f**). Bar, 20 μm. (**B**) Pull-down assays of Flag-tagged and endogenous EPLIN and endogenous KIF14 with GST-tagged supervillin fusion proteins. SDS-PAGE gels were loaded with the input HeLa lysate (lanes 1) and the bound and unbound fractions after sedimentation with GST only (lanes 2), GST-SV1009-1398 (lanes 3), or GST-SV1398-1792 (lanes 4).

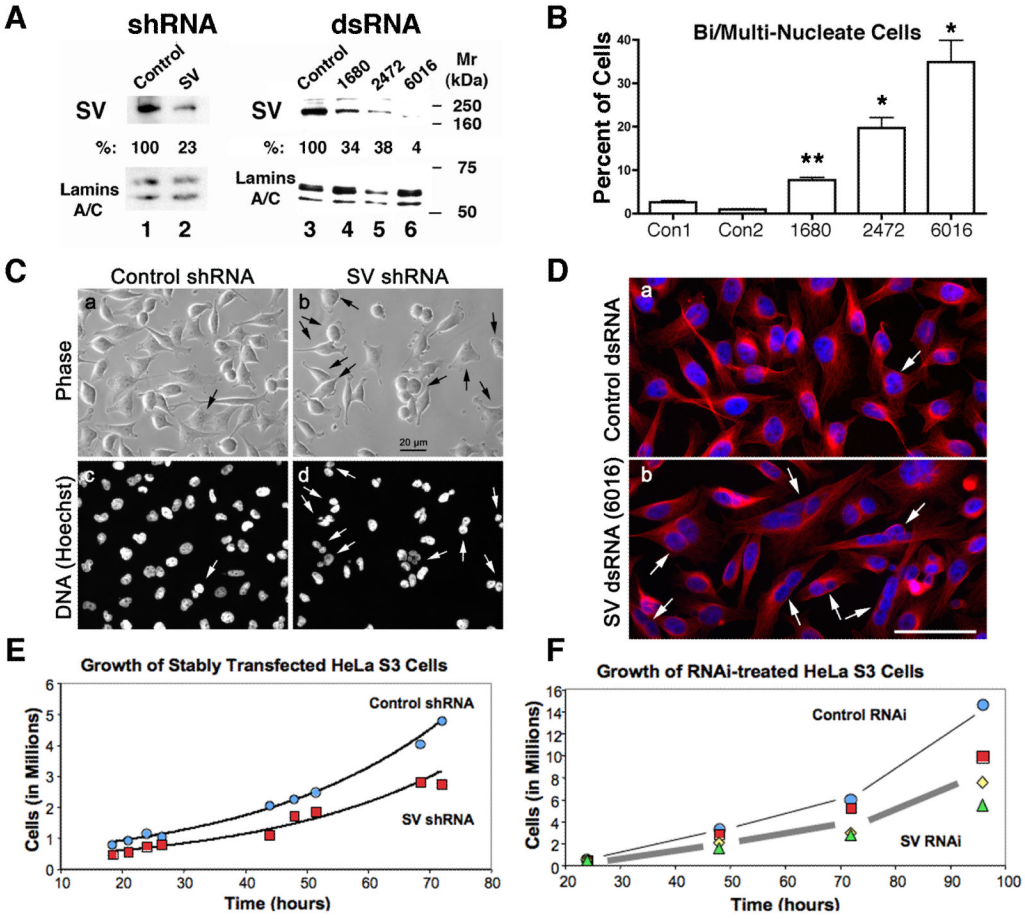

Fig. 7.

Supervillin (SV) is required for normal cell division. (**A**) Immunoblots showing the percentages (**%**) of endogenous supervillin remaining in HeLa cells with a stably incorporated control (lane 1) or supervillin-specific (lane 2) shRNA or after treatment with a control dsRNA (lane 3) or a dsRNA targeting each of 3 supervillin sequences (lanes 4-6). Percentages were calculated after normalizing the supervillin signals to the lamin A/C loading controls. (**B**) The percentages of HeLa cells containing 2 or more nuclei/cell were scored 72 hr after a single transfection with 20 nM dsRNA against human supervillin nucleotides 1680, 2472, 6010 or with control RNAi corresponding to scrambled sequences for 1680 (Con1) or 2472 (Con2). Means of three experiments shown with standard deviation; p values: * < 0.03, ** = 0.0058, using two-tailed unpaired t-test with Welch correction. (**C**) Phase-contrast (**a, b**) and fluorescence (**c, d**) micrographs of puromycin-selected HeLa cells containing either a control (**a, c**) or a supervillin-specific (**b, d**) shRNA after fixation and staining for DNA with Hoechst dye. (**D**) DNA (blue) and phalloidin-stained actin in cytoplasm (red) of HeLa cells 3 days after treatment with 20 nM of either Con1 control (**a**) or 6016 (**b**) dsRNA. (**C, D**) **Arrows**, bi- and multi-nucleate cells. Bars, 20 µm. (**E**) Growth rates of HeLa cells that stably express a control (●) or supervillin-specific (■) shRNA (n = 1). (**F**) Growth rates also are reduced by RNAi against SV nucleotides 1680 (■), 2472 (◆), and 6016 (▲), as compared with a similar treatment with control RNAi (●, Con1). Representative of 3–5 experiments/siRNA.

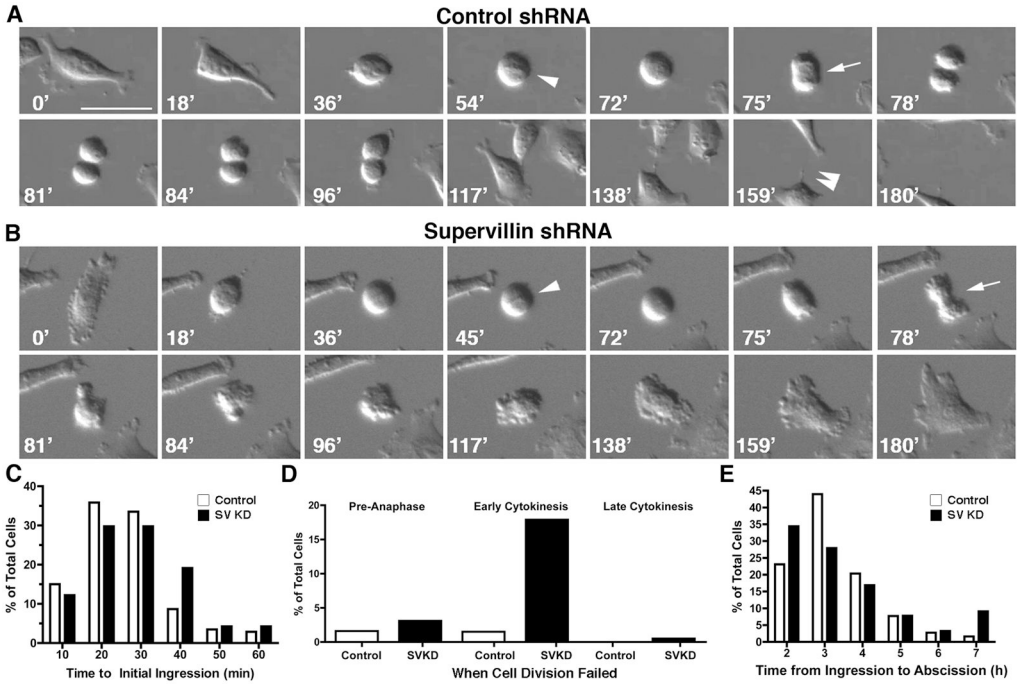

Fig. 8.

Cytokinesis failure in supervillin-knockdown cells occurs primarily during furrow ingression. Unsynchronized HeLa cells were treated with (**A**) control or (**B**) the supervillin-specific 6016 RNAi for 48 hr and then imaged every 3 min for 16–24 hr. Elapsed times are given in minutes with the initial image set at time (t) = 0. Bar, 100 μm. **Arrowheads**, metaphase plates; **arrows**, first membrane ingression; and **double arrowhead**, intracellular bridge. (**C**) The time from chromosome alignment at the metaphase plate to the appearance of the first furrow was not significantly longer for supervillin knockdown cells (**black bars**, n = 187) than for controls (**white bars,** n = 172). (**D**) Few cells treated with control RNAi (**white bars,** n = 201) failed at either chromosome separation (pre-anaphase) or during cytokinesis; most supervillin-depleted cells (**black bars**, n = 200) that failed cytokinesis did so during the initial furrow formation in early cytokinesis. (**E**) For cells completing cytokinesis, no significant difference was observed in the time between the initial furrow ingression and breakage of the intracellular bridge for control (**white bars,** n = 181) and supervillin knockdown (**black bars**, n = 153) cells.

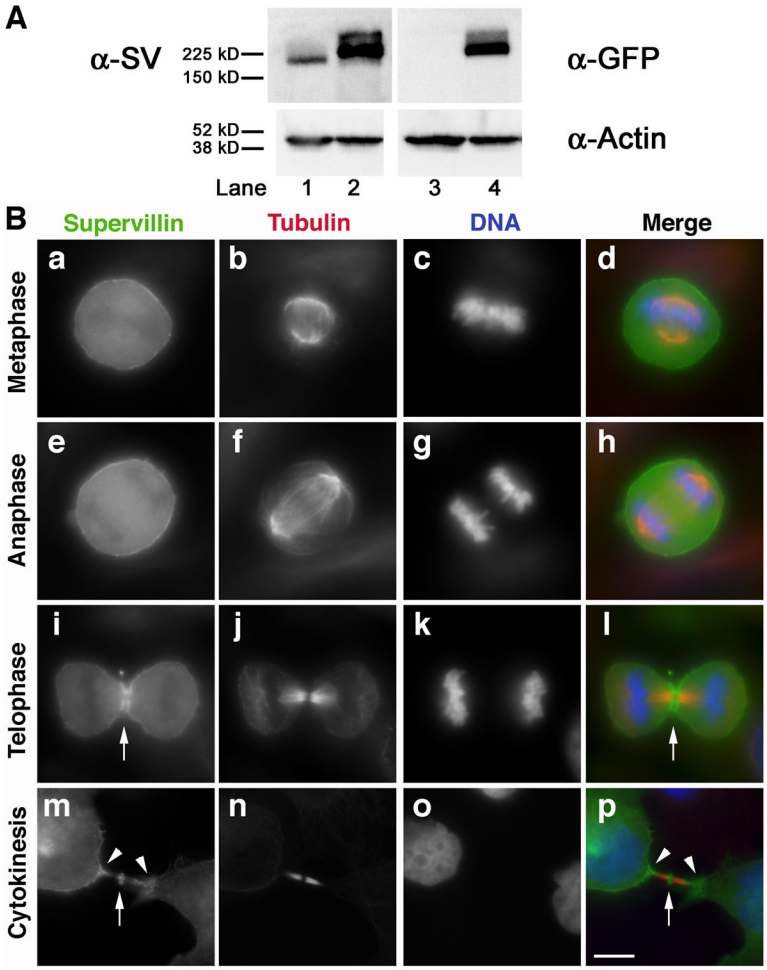

Fig. 9.

Supervillin concentrates at the cleavage furrows and midbodies of dividing cells. (**A**) **Upper panel**, immunoblots stained with antibody against supervillin (**lanes 1, 2**) or GFP (**lanes 3, 4**) of whole cell lysates from untransfected HeLa cells (**lanes 1, 3**) and HeLa cells stably expressing EGFP-tagged human supervillin (**lanes 2, 4**). Lower panel,β-actin loading control. (**B**) Wide-field immunofluorescence micrographs of synchronized HeLa cells during mitosis were stained for stably expressed EGFP-supervillin with anti-EGFP (**a, e, i, m; green in merges**), endogenous tubulin (**b, f, j, n; red in merges**) and DNA (**d, h, l, p; blue in merges**). Arrows show staining at the cleavage furrow (**i, l**) and abscission site in the midbody (**m, p**); arrowheads denote localizations at the extremities of an intracellular bridge (**m, p**). Bar, 10 μm.

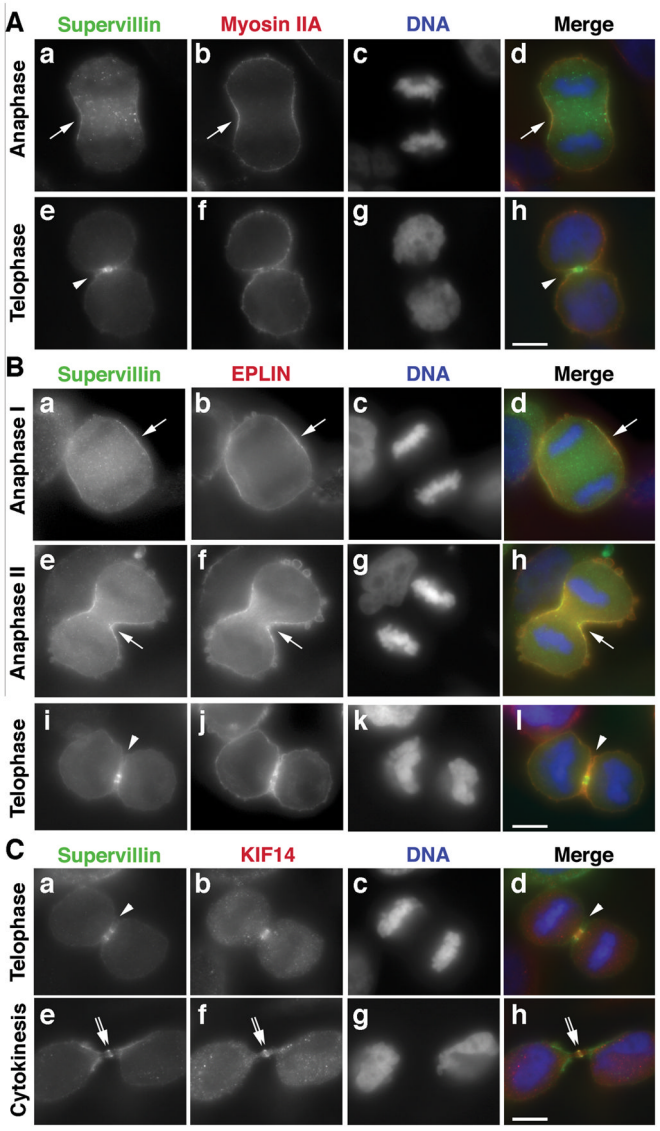

Fig. 10.

Supervillin overlaps with myosin IIA and EPLIN at the cleavage furrow and with KIF14 at the midbody. Wide-field immunofluorescence micrographs of synchronized HeLa cells during mitosis were stained for stably expressed EGFP-supervillin with anti-EGFP, as noted (**green in merges**); for endogenous (**A**) myosin IIA, (**B**) EPLIN, or (**C**) KIF14 (**red in merges**); and DNA (**blue in merges**). Arrows show overlaps at the cleavage furrow; arrowheads denote supervillin concentrations at the midbody; and double arrows mark staining of the abscission site in the midbody. Bars, 10 μm.

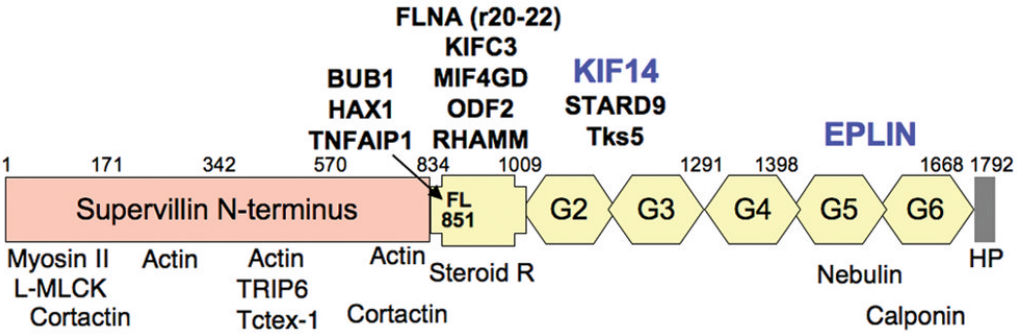

Fig. 11.

Localizations of new candidate interactors (**top, bolded**) along the supervillin amino acid sequence. Supervillin residues Phe-851 and Leu-852 are required for interactions with BUB1, HAX1, and TNFAIP1. DN-RHAMM and supervillin-binding fragments of the new interactors induce supervillin mis-localization within mammalian cells. The association of supervillin with full-length, endogenous KIF14 and EPLIN (**blue**) have been confirmed by GST pull-down. Three of these fragments correspond to non-motor domains of kinesins (KIF14, KIFC3) or a kinesin-like protein (STARD9). Previously reported binding partners for supervillin are shown below the structural schematic. These include the myosin II heavy chain, L-MLCK, cortactin, actin, TRIP6, Tctex-1, nebulin, calponin, and steroid receptors that bind to androgen (AR), estrogen (ERα), glucocorticoids (GR), and peroxisome proliferators (PPAR-γ).

Table 1

Potential binding partners for the supervillin C-terminus

Positive interactors for supervillin sequences were identified in untargeted yeast two-hybrid assays and screened for interactions with bait constructs in directed assays for leucine autotrophy and β-galactosidase activity.

SV834-1291 preys	Genbank #		Residues in prey vectors:	No. of clones (d1, d2, d3, d4; Ind)	Directed Y2H results:			Prey contains coiled coil
					SV834-1291	SV1008-1791	SV834-1291, F851S, L852P	
KRT18	NM_199187	NP_954657	98–243, 130–385	3, 0, 0, 0; 2	++	−	−	✓
*MIF4GD (hSLIP1)	NM_020679	NP_065730	122–256	1, 0, 0, 0; 1	++	−	++	
*ART-27 (UxtV2)	NM_004182	NP_004173	1–157 (FL)	1, 0, 0, 0; 1	++	−	−	−
ITGB3BP (NRIF3)	NM_014288	NP_055103	12–161	1, 0, 0, 0; 1	++	−	++	
*BUB1	NM_004336	NP_004327	4–313	1, 0, 0, 0; 1	++	−	−	−
*CENPF	NM_016343	NP_057427	2378–2516	1, 0, 0, 0; 1	++	−	++	
*FLNA (rpts20-22)	NM_001456	NP_001447	2169–2414	1, 0, 0, 0; 1	++	−	++	
*HAX1 (HS1BP1)	NM_006118	NP_006109	144–279	1, 0, 0, 0; 1	++	−	−	−
HSP90	NM_005348	NP_005339	11–241	1, 0, 0, 0; 1	++	−	++	
*KIFC3	NM_005550	NP_005541	237–366	1, 0, 0, 0; 1	++	−	++	
LMNA	NM_170707	NP_733821	221–448	1, 0, 0, 0; 1	++	−	−	✓
LMNB2	NM_032737	NP_116126	161–342	1, 0, 0, 0; 1	++	−	−	✓
MPHOSPH9	NM_022782	NP_073619	673–858	1, 0, 0, 0; 1	++	++	++	
*NM23B (NME2)	NM_002512	NP_002503	1–152	1, 0, 0, 0; 1	++	−	++	
*ODF2 (Cenexin)	NM_153437	NP_702915	133–269	1, 0, 0, 0; 1	++	−	++	
PAN3	NM_175854	NP_787050	229–600	1, 0, 0, 0; 1	++	−	−	−
PCNXL3	NM_032223	NP_115599	365–548	1, 0, 0, 0; 1	++	−	++	
*RHAMM (HMMR)	NM_012485	NP_036617	295–422	1, 0, 0, 0; 1	++	−	++	
*TNFAIP1	NM_021137	NP_066960	119–316	1, 0, 0, 0; 1	++	−	−	−
SV1008-1791 preys								
*EPLINβ (LIMA1)	NM_016357	NP_057441	672–759, 650–759	0, 1, 7, 4; 2	−	++	na	
*ATRX	NM_000489	NP_000480	97–292	0, 0, 1, 1; 1	++	++	na	
*KIF14	NM_014875	NP_055690	1522–1648	0, 0, 1, 0; 1	++	++	na	
MKL2	NM_014048	NP_054767	382–692	0, 0, 1, 0; 1	++	++	na	
MLL	NM_005933	NP_005924	968–1206	0, 0, 1, 0; 1	++	++	na	
*Tks5 (Fish, SH3MD1)	NM_014631	NP_055446	337–488, 318–655	0, 0, 0, 5; 2	++	++	na	

SV834-1291 preys	Genbank #		Residues in prey vectors:	No. of clones (d1, d2, d3, d4; Ind)	Directed Y2H results:			Prey contains coiled coil
					SV834-1291	SV1008-1791	SV834-1291, F851S, L852P	
MPHOSPH9	NM_022782	NP_073619	673–858, 809–1031	0, 0, 0, 2; 2	++	++	na	
*FLNA (rpts8-10)	NM_001456	NP_001447	987–1186	0, 0, 0, 1; 1	++	+	na	
KIF22	NM_007317	NP_015556	488–665	0, 0, 0, 1; 1	+	++	na	
*STARD9	*XM_001129482*	*XP_001129482*	2528–2663	0, 0, 0, 1; 1	++	++	na	

Preys marked with an asterisk (*) co-localized with EGFP-supervillin after co-expression in COS7-2 cells. The names, nucleic acid and protein accession numbers, amino acid residues encoded by the prey vectors, the numbers of colonies containing each interactor identified on day 1 (d1) through day 4 (d4), and the numbers of independent clones (Ind.) are shown. Directed assays were carried out with the bait vectors SV834-1291 and SV1008-1791, to confirm the undirected results and delimit the regions of interest. To test for interactions dependent on potential coiled-coil associations, directed assays also were performed with the SV834-1291 bait carrying mutations at amino acids L952H and L953P (not shown) or at F851S and L852P: ++, passed both tests for positive interaction; +: passed one test only, **na**: not assayed. Three of the preys with disrupted interactions also contain predicted coiled coils (✔).

Table 2

Probable functional supervillin (SV) interactors

Summary of prey sequence co-localization with and mis-localization of supervillin (columns 1–3), the conservation among mammalian sequences of the supervillin-interacting (**SV-I**) site (column 4), and known functions of the full-length prey proteins (columns 5–9). The extents of the co-localizations of prey fragments with supervillin were scored as high (**H**), medium (**M**), or low (**L**) at intracellular punctae (**P**), the cell edge (**E**), and/or fibers (**F**), as shown in previous figures. Due to cloning difficulties, wild-type RHAMM was used to assess co-localization and dominant-negative RHAMM was assayed for mis-localization. The relative conservation of the supervillin-interacting site was assessed by CLUSTALW alignments of predicted amino acid sequences from the human, murine, bovine, canine, equine, and opossum or rat genomes.

Supervillin (SV) Interactor	Co-Localization	Shifts SV to	Conservation of SV-I Site	Cell Motility	Membrane Trafficking	ERK Signaling	Cancer-related	Cell Division
EPLIN/LIMA1	**H (P, E)**	**E**	+++	✓		✓	**Suppressor**	✓
KIF14	**H (P, E)**	**P**	+				**Oncogene**	✓
KIFC3	**H (E, F)**	**E**	+++		✓			
TNFAIP1	**H (P)**	**P**	+++			**?**		
BUB1	**M (P, F)**	**P**	++			✓	✓	✓
HAX1	**M (P, E)**	**P**	++	✓	✓	✓	✓	
STARD9/KIF16A	**M (E)**	**P**	**?**		**?**			
Tks5/SH3PXD2A	**M (E)**	**P**	+++			✓	**Invasion**	
TRIP6 (control)	M (P)	P	+++	✓		✓	Invasion	
FLNA, rpt 20–22	**L (P, E)**	**P**	+++	✓	✓	✓	✓	
MIF4GD/SLIP1	**L (P)**	**P**	+++					
ODF2/Cenexin	**L (E)**	**P**	+++				**?**	✓
RHAMM	**L (P)**	**E**	++	✓		✓	**Oncogene?**	✓